

**Study of Hydrogen Bonded Complexes
between Formic Acid and Phenylacetylene using
Matrix Isolation Infrared Spectroscopy and Computations**

Gaurav Kumar

*A dissertation submitted for the partial fulfillment of
BS-MS dual degree in Science*



**Indian Institute of Science Education and Research Mohali
April 2013**

Certificate of Examination

This is to certify that the dissertation titled “Study of Hydrogen Bonded Complexes between Formic Acid and Phenylacetylene using Matrix Isolation Infrared Spectroscopy and Computations” submitted by Mr. Gaurav Kumar (Reg. No. MS08022) for the partial fulfillment of BS-MS dual degree programme of the Institute, has been examined by the thesis committee duly appointed by the Institute. The committee finds the work done by the candidate satisfactory and recommends that the report be accepted.

Dr. Sanjay Mandal

Dr. K. R. Shamsunder

Prof. K.S. Viswanathan
(Supervisor)

Dated: April 26, 2013

DECLARATION

The work presented in this dissertation has been carried out by me under the guidance of Prof. K. S Viswanathan at the Indian Institute of Science Education and Research Mohali.

This work has not been submitted in part or in full for a degree, a diploma, or a fellowship to any other university or institute. Whenever contributions of others are involved, every effort is made to indicate this clearly, with due acknowledgement of collaborative research and discussions. This thesis is a bonafide record of original work done by me and all sources listed within have been detailed in the bibliography.

Gaurav Kumar

(Candidate)

Dated: April 26, 2013

In my capacity as the supervisor of the candidate's project work, I certify above statements by the candidate are true to the best of my knowledge.

Prof. K.S. Viswanathan

(Supervisor)

ACKNOWLEDGEMENT

I express my deep sense of gratitude and profound feeling of admiration to Prof. K. S. Viswanathan for his advice, expert guidance, valuable suggestions, discussions and constant encouragement during the entire course of this work and preparation of the thesis. I have really enjoyed the work under his guidance.

I am also grateful to my Master's thesis committee members Dr. Sanjay Mandal and Dr. K. R. Shamsunder for their valuable suggestions and comments during the committee meeting.

I have no words to express my gratefulness to Dr. Bishnu Prasad Kar for his invaluable help, discussions in the lab during the setting-up the facility and sustained encouragement. I am also grateful to my lab members Kapil and Ginny, who accompanied me throughout this research work.

I owe a special word of thanks to Sumit Mittal, Asif Equbal and Pradeep Kumar for helping me in carrying out the computational calculations.

I thank each of my classmates who provided a wonderful and friendly atmosphere to carry out research during the entire period. It is my pleasure to thank each and every member of the Department of Chemical sciences who have helped me in various ways during the course of investigation and research.

I wish to acknowledge the Computing Facility staff for providing me excellent facilities during the computational work. I am extremely thankful to Prof. N. Sathyamurthy, Director, IISER Mohali, for allowing me to use the various facilities of this institute to carry out the research work.

I express my sincere gratitude to each of my family members for their encouragement and moral support throughout the course of study.

I would also like to acknowledge the 'Department of Science and Technology, India' for providing the INSPIRE fellowship.

LIST OF FIGURES

Figure	Figure Caption	Page No
Figure 1	(a) Phenylacetylene, (b) Formic acid indicating the hydrogen bonding sites	10
Figure 2	Potential energy curves for a polyatomic molecule trapped in a matrix	16
Figure 3	Photograph of the Matrix Isolation IR spectroscopy set-up	19
Figure 4	Main Components of Matrix Isolation IR spectroscopy set up	20
Figure 5	Photograph of compressor and chiller	22
Figure 6 (a)	Block diagram of the internal structure	23
Figure 6 (b)	Steps 1 and 2 of the Gifford-McMahon cycle	24
Figure 6 (c)	Steps 3 and 4 of the Gifford-McMahon cycle	24
Figure 7	IR spectra of water at 12 K	34
Figure 8 (a)	Computed spectrum of Complex 1 at M06-2X/6-311++G (d, p); Scale : (4000 -400 cm ⁻¹)	46
Figure 8 (b)	Computed spectrum of Complex 1 at M06-2X/6-311++G (d, p); Scale: (4000 – 3000 cm ⁻¹)	47
Figure 8 (c)	Computed spectrum of Complex 1 at M06-2X/6-311++G (d, p); Scale: (2000 – 1000 cm ⁻¹)	47
Figure 9 (a)	Computed IR spectra of the Complex 1* at B3LYP/6-311++G(d,p); Scale: (4000 – 400 cm ⁻¹)	49
Figure 9 (b)	Computed IR spectra of the Complex 1* at B3LYP/6-311++G(d,p); Scale: (3850- 2850)	50
Figure 9 (c)	Computed IR spectra of the Complex 1* at B3LYP/6-311++G(d,p); Scale: (2000 – 1000 cm ⁻¹)	50
Figure 10 (a)	Spectrum of phenylacetylene recorded in liquid state and in matrix; Scale: (3500-3000 cm-1)	52
Figure 10 (b)	Spectrum of phenylacetylene recorded in liquid state and in matrix; Scale: (1600-1000 cm-1)	53
Figure 11	Optimized geometry of Complex 1 at M06-2X/6-311++G (d, p)	55

LIST OF TABLES

Table	Table Heading	Page No
Table 1	Some properties of very strong, strong and weak hydrogen bonds	6
Table 2	Optimized geometries of different complexes at different levels calculation	35-37
Table 3	Computed stabilization energy of the complexes at M06-2X/6-311++G (d, p) level	39
Table 4	Computed stabilization energy of the complexes at MP2/6-311++G (d, p)	39
Table 5	Computed stabilization energy of the complexes at B3LYP/6-311++G (d, p)	40
Table 6	Computed frequencies of the monomers and complexes at M06-2X/6-311++G (d, p)	42
Table 7	Computed frequencies of the monomers and complexes at MP2/6-311++G (d, p)	43
Table 8	Computed frequencies of the monomers and complexes at B3LYP/6-311++G (d, p)	44
Table 9	Computed frequencies of the monomers and complexes at B3LYP/6-311++G (d, p)	45
Table 10	Some selected geometrical parameters at M06-2X /6-311++G (d, p)	54

LIST OF NOTATIONS

PhA	Phenylacetylene
FA	Formic acid
FT	Fourier Transform
AC	Acetylene
UV	Ultra Violet
Elec	Electrostatic
Ind	Inductive
Dis	Dispersive
Rep	Repulsive
GM	Gifford-McMahon
KBr	Potassium Bromide
HF	Hartree-Fock
MP	Møller–Plesset perturbation theory
DFT	Density Functional Theorem
CI	Configuration interaction
CC	Coupled cluster
MRCI	Multi-reference configuration interaction
BLYP	Becke-Lee-Yang-Parr
SCF	Self- Consistent Field
M06	Minnesota functional
GGA	Generalized Gradient Approximation
FWHM	full width at half maximum
ZPE	Zero point vibrational energy
BSSE	Basis Set Superposition Error
AIM	Atoms –in-molecules
CP	Critical point

Contents

	Page No.
List of Figures	i
List of Tables	ii
List of Notations	iii
Abstract	vi
Chapter 1 Introduction	1
1.1 The hydrogen bond	2
1.1.1 Historical Background	2
1.1.2 Definition of a hydrogen bond	3
1.1.3 Criteria for the formation of a hydrogen bond	3
1.1.4 Some characteristics of hydrogen bonds	4
1.2 Classification of a hydrogen bond	4
1.3 Methods of studying weak hydrogen bonding	5
1.3.1 Diffraction methods	5
1.3.2 Vibrational Spectroscopy	5
1.3.3 Gas-phase rotational spectroscopy	5
1.3.4 Computation	7
1.4 Status of current research in weak hydrogen bonded interaction	7
1.5 Motivation for the present work	9
1.6 Scope and objective of the present work	11
Chapter 2 Experimental and Computational Procedures	12
2.1 Matrix Isolation Technique	12
2.2 Advantages	13
2.3 Matrix environmental effects	13
2.3.1 Multiple trapping sites	13
2.3.2 Molecular Rotation	14
2.3.3 Aggregation	14
2.3.4 Matrix shifts	14

2.4	Characteristics of matrix materials	15
2.4.1	Inertness	17
2.4.2	Rigidity	17
2.4.3	Transparency	17
2.4.4	Volatility	17
2.4.5	Latent heat of Fusion and thermal conductivity	17
2.5	Matrix Structure	18
2.6	Equipment	18
2.6.1	Cryostat based on a closed cycle helium Compressor	21
2.6.2	Vacuum system	25
2.6.3	FTIR spectrometer	26
2.6.4	Sample Introduction system	26
2.7	Experimental procedure	26
2.8	Computational Procedure	26
2.8.1	Geometry optimization and frequency calculation	28
2.8.2	Stabilization energy calculation of complexes	29
2.8.3	Atoms –in-molecules (AIM) methodology	30
Chapter 3	Results and Discussions	32
3.1	Introduction	32
3.2	Computational details	32
3.3	Experimental details	33
3.4	Results and Discussions	33
3.5	Vibrational Analysis	41
3.6	Geometrical parameters	51
Chapter 4	Conclusion	56
	Bibliography	58
	Poster Presentations / Publications	61

Abstract

Weak interactions, particularly hydrogen bonding interactions, play an important role in many biological and chemical systems. Most of the bio-molecular conformations are maintained by the hydrogen bonding.

There are many experimental techniques, which have been used to study weak interactions. One such technique is matrix isolation infrared spectroscopy, which serves as a powerful tool to explore weak interactions and conformations. The sharp spectral feature obtained in matrix isolation technique permits the resolution of features due to weak complexes and different conformations.

Hydrogen bonding has been extensively studied in last two decades. In recent times, weak hydrogen bonding such as O-H $\cdots\pi$ and C-H $\cdots\pi$ has drawn considerable attention. Another interesting aspect is the investigation of competitive hydrogen bonding in a molecule with multiple bonding sites.

Formic acid and phenylacetylene are two ideal examples having multiple hydrogen bonding sites. Both can act as proton donor and proton acceptors, which eventually gives rise to a number of hydrogen bonded systems for these two precursor molecules.

In this thesis, the hydrogen bonded complexes of formic acid and phenylacetylene have been studied. The main aim of this work is to elucidate the structures of the various hydrogen bonded complexes between the two precursor molecules. The computational work has been performed at M06-2X, MP2 and B3LYP level of theory using 6-311++G (d, p) basis set. Fourteen different geometries at the M06-2X, twelve at MP2 and thirteen at B3LYP level were obtained. Most of the structures at the different levels are similar at all three levels. The O-H $\cdots\pi$ interaction has been observed as a dominating interaction computationally in the ground state optimized at all three levels. To study these complexes experimentally, the matrix isolation experimental facility has been set up.

Chapter 1

Introduction

This chapter discusses the studies on hydrogen bonding and places the present work in context. The computational and experimental methods described in the literature to study hydrogen bonding have also been discussed.

Types of intermolecular bonds:

There are four basic types of intermolecular bonds formed between two or more molecules, ions, or atoms. Intermolecular interactions cause molecules to be attracted or repelled by each other in order to attain the maximum stability. These interactions are also responsible for the physical characteristics of the substance [1].

- **Dipole-Dipole interactions:** In molecular species, a permanent charge separation, or dipole will be observed if two bonded atoms are significantly different in electronegativity. Two molecular species with permanent dipoles can interact through dipole-dipole interactions.
- **London-Dispersion Force:** It arises due to instantaneous dipoles in neighbouring atoms formed by charge imbalance. Since the negative charge of the electron is not uniform around the whole atom, there will always a tendency of charge imbalance. The small charge will induce a corresponding dipole in a nearby molecule; causing an attraction between the two.
- **Hydrogen Bond:** A hydrogen bond is effectively a strong example of an interaction between two permanent dipoles. The large difference in electronegativities between hydrogen and any of fluorine, nitrogen and oxygen, coupled with their lone pairs of electrons cause strong electrostatic forces between molecules. Hydrogen bonds are responsible for the high boiling points of water and ammonia compared with their heavier analogues.
- **Cation- π interaction:** It occurs between a π bond and a cation.

We will discuss in some detail the hydrogen bonding system which is the prime interaction that is expected to be present in the complexes in this study.

1.1 The hydrogen bond:

The hydrogen bond is a unique type of a bond in structural chemistry and biology, and plays an important role in molecular association. Its functional importance arises from both thermodynamics and kinetics considerations. In supramolecular chemistry, the hydrogen bond controls and directs the molecular assemblies due to its strength and directionality. The strength of the hydrogen bond lies between the van der Waals interactions and covalent bonds, which therefore allows hydrogen bonds to associate and dissociate quickly at ambient temperatures. This ability allows the hydrogen bond interaction to achieve specificity of recognition in a short time interval, which is a necessary criterion for biological reactions to occur at room temperature.

In that first, 1939 edition of *The Nature of the Chemical Bond*, Pauling introduces the hydrogen bond in the following words [2]:

“Although the hydrogen bond is not a strong bond (its bond energy, that is the energy of the reaction $XH=Y \rightarrow XHY$, being only about 5kcal/mole), it has great significance in determining the properties of substances. Because of its small bond energy and the small activation energy involved in its formation and rupture, the hydrogen bond is especially suited to play a part in reactions occurring at normal temperatures. It has been recognized that hydrogen bonds restrain protein molecules to their native configurations, and I believe that as the methods of structural chemistry are further applied to physiological problems it will be found that the significance of the hydrogen bond for physiology is greater than that of any other single structural feature”.

For these reasons, the area of hydrogen bonding has fascinated chemists and biologists from several decades and is now central to chemistry and biology.

1.1.1 Historical Background:

The earliest references of the concepts regarding the hydrogen bonds occur in the German literature and in a publication [3] *“The state of amines in aqueous solution”*. In 1920, Latimar and Rodebush suggested that ‘a free pair of electrons on one water molecule might be able to exert sufficient force on a hydrogen held by a pair of electrons

on another water molecule to bind the two molecules together' and that 'the hydrogen nucleus held between two octets constitutes a *weak bond*'. In 1935, Linus Pauling used the term 'hydrogen bond' for the first time and freely to account for the residual entropy of ice. Pauling was clear and unambiguous in the use of the word *bond* when he stated that under certain conditions an atom of hydrogen is attracted by rather strong forces to two atoms, instead of only one, so that it may be considered to be acting as a bond between them [4].

1.1.2 Definition of a hydrogen bond:

An accurate definition of the hydrogen bond remained ambiguous for a long time. The original definition of a hydrogen bonding invoked two electronegative atoms (X and Y) interacting through a hydrogen atom as in $X-H\cdots Y$. Initially X and Y were found to be mostly N, O and F which led to the mentioning of these atoms as part of the definition of hydrogen bonds in various sources or literatures. In 2011, a task group formed by IUPAC, consisting of 25 experts all over the world, has given the modern definition of the hydrogen bonding [5].

“The hydrogen bond is an attractive interaction between a hydrogen atom from a molecule or a molecular fragment $X-H$ in which X is more electronegative than H, and an atom or a group of atoms in the same or a different molecule, in which there is evidence of bond formation”.

A typical hydrogen bond is denoted as $X-H\cdots Y-Z$, where the bond is depicted by three dots. $X-H$ represents the hydrogen bond donor. The acceptor may be an atom or an anion Y, or a fragment or a molecule $Y-Z$, where Y is bonded to Z. In some special cases, X and Y are the same leading to symmetric hydrogen bonds, since $X-H$ and $Y-H$ distances become equal. In any situation, the acceptor is an electron rich region such as lone pair of Y or π -bonded pair of $Y-Z$. There are some criteria and characteristics which need to be fulfilled to be considered as a hydrogen bond. The greater the number of criteria satisfied, the more definitive is the characterization of a hydrogen bond.

1.1.3 Criteria for the formation of a hydrogen bond

For a hydrogen bond $X-H\cdots Y-Z$

- The forces involved in the formation of a hydrogen bond are usually electrostatic in

nature. They arise from charge transfer between the donor and acceptor leading to partial covalent bond formation between H and Y, and from dispersion forces.

- The atoms X and H are covalently bonded to one another and the X–H bond is polarized during the formation of the hydrogen bond, with the H···Y bond strength increasing with the increase in electronegativity of X.
- The X–H···Y angle is usually linear (180°) and the closer the angle is to 180° the stronger is the hydrogen bond.
- The length of the X–H bond usually increases on hydrogen bond formation with a consequent red shift in the infrared X–H stretching frequency and an increase in the infrared absorption cross-section for the X–H stretching vibration. The greater the lengthening of the X–H bond in X–H···Y, the stronger is the H···Y bond. Simultaneously, new vibrational modes associated with the formation of the H···Y bond are also generated.
- The X–H···Y–Z hydrogen bond leads to characteristic NMR signatures that typically include pronounced proton deshielding for the H in X–H.
- The Gibbs energy of formation for the hydrogen bond should be greater than the thermal energy of the system for the hydrogen bond to be detected experimentally.

1.1.4 Some characteristics of hydrogen bonds:

- The pK_a of X–H and pK_b of Y–Z in a given solvent correlate strongly with the energy of the hydrogen bond formed between them.
- Hydrogen bonds show directional property and influence packing modes in crystal structures.
- Estimates of charge transfer in hydrogen bonds show that the interaction energy correlates well with the extent of charge transfer between the donor and the acceptor.
- Analysis of the electron density topology of hydrogen-bonded systems usually shows a bond path connecting H and Y associated with (3,–1) bond critical point between H and Y.

1.2 Classification of a hydrogen bond:

There is no clear cut division between very strong, strong and weak hydrogen bonding. Based on the different properties which include geometric, energetic, thermodynamic, and functional aspects, we can tabulate the hydrogen bonding into

certain categories. **Table 1** lists properties of a hydrogen bond that we classify as very strong, strong and weak. The table is meant to be used as a guide only [4] and cannot be considered to be definitive.

1.3 Methods of studying weak hydrogen bonding:

There are various instrumental and computational techniques, which can be implemented to study the weak hydrogen bonds. These include diffraction methods, vibrational spectroscopy, gas phase rotational spectroscopy and computations. Each of these techniques has been briefly described below.

1.3.1 Diffraction methods:

Weak hydrogen bonds can be easily detected by diffraction technique as compared to spectroscopic ones. Neutron diffraction is closely associated with the field of hydrogen bonding because only with this technique crystallographers can establish the position of the most crucial atom in the interaction accurately, namely hydrogen. This technique is of unusual importance in the study of hydrogen bonding to multi-atom π -bases, where it is not possible to infer the H-atom positions on the basis of geometrical considerations. The advances in low temperature technique coupled with X-ray diffraction have also proven to be invaluable.

1.3.2 Vibrational Spectroscopy:

It is a classical method for the study of hydrogen bonding in condensed phases. Its applicability ranges from strongest to weakest hydrogen bond types, both in solution and the solid state. The probe here is the vibrational frequencies of the atomic groups involved in the hydrogen bonding. Relatively small shifts, say around $5\text{-}20\text{ cm}^{-1}$, in the X-H stretching frequency with respect to the free molecule, is considered an evidence for the formation of a hydrogen bond. Cold molecules techniques such as molecular beams and matrix isolation have proven to be invaluable for the study of hydrogen bonding systems.

1.3.3 Gas-phase rotational spectroscopy:

The technique probably provides the most accurate information of the structure of the gas phase hydrogen bonded adducts. The experiments are conducted using cold molecular beams. Adducts can be observed in the ground vibrational state, free from any other molecular interference. Apart from geometries, dissociation energies, force

Table 1 - Some properties of very strong, strong and weak hydrogen bonds

	Very strong	Strong	Weak
Bond energy (-kcal/mol)	15-40	4-15	<4
Examples	$[F\cdots H\cdots F]^-$, $[N\cdots H\cdots N]^+$, P^- $OH\cdots O=P$	$O-H\cdots O=C, N^-$ $H\cdots O=C, O-H\cdots O-H$	$C-H\cdots O, O-H\cdots \pi$
IR ν_s relative shift	>25%	5-25%	<5%
Lengthening of X-H(Å)	0.05-0.2	0.01-0.05	<0.01
D(H \cdots A) range (Å)	1.2-1.5	1.5-2.2	2.0-3.0
$\Theta(X-H\cdots A)$ range(°)	175-180	130-180	90-180
KT (room temperature)	>25	7-25	<7
Effect on crystal packing	Strong	Distinctive	Variable
Covalency	Pronounced	Weak	Vanishing
Electrostatics	Significant	Dominant	Moderate

constants and other parameters may also be derived [6]. This kind of information is of fundamental importance because it cannot be obtained from experiments in condensed phases where the equilibrium geometry is not directly observable.

1.3.4 Computation:

Computational chemistry serves to provide excellent complimentary information to corroborate spectroscopic and crystallographic data in the study of weak intermolecular interactions. Theoretical methods can provide benchmark values for the energies of intermolecular interactions without any complicating effects of the solvent or solid state environment. Computational methods can also be used to study the domains of the potential energy surface which are far from the equilibrium structure [7]. Because of the widespread availability of powerful and low-cost computers and availability of efficient computer implementations, theoretical methods are now accessible to a large number of structural chemists. Theory coupled with database research has emerged as an effective way of studying weak intermolecular interactions.

Among the methods described above, we propose to use matrix isolation infrared spectroscopy to study the hydrogen bonded complexes between phenylacetylene (PhAc) and formic acid (FA).

Matrix isolation infrared spectroscopy has been extensively used to study molecular interactions and conformational isomerism. One of the primary advantages of this technique is the narrow bandwidth that it provides which permits the resolution of bands which are otherwise overlapped in the condensed phases and to a certain extent in the vapour phase. The use of a Fourier Transform Infrared (FTIR) spectroscopy in conjunction with the matrix isolation technique, makes it possible to identify adduct formation and to measure accurately the frequency of the infrared bands.

A detailed description of the technique is provided in Chapter 2.

1.4 Status of current research in weak hydrogen bonded interaction

Conventional strong hydrogen bonds such as $\text{OH}\cdots\text{O}$, $\text{NH}\cdots\text{O}$, and $\text{OH}\cdots\text{N}$ have been well studied. The weak or nonconventional hydrogen bonding, such as $\text{CH}\cdots\text{O}$ and $\text{H}\cdots\pi$ interactions, are of considerable interest in recent years because of their significant role in determining the shapes and stabilities of proteins and crystal structures. There are many experimental and theoretical studies of $\text{C-H}\cdots\text{X}$ complexes, where X can be various proton acceptors such as O, N, halogens, and π systems. The matrix isolation technique

has been extensively used to study the hydrogen-bonded complexes of alkynes and alkenes with several oxygen and nitrogen bases by Ault and co-workers [8, 9].

Hydrogen-bonded complexes of $Y-H\cdots\pi$, in which the hydride acts as proton donor towards the π system of benzene-, acetylene-, or ethylene-type systems, were also investigated by many authors [10].

Sander et al. [11] has also performed similar work by matrix isolation infrared and ab initio study of hydrogen bonds formed between acetylene and formic acid. In this system, $O-H\cdots\pi$ and $C_{(AC)}-H\cdots\pi$ were the two dominating hydrogen bonding interactions. The ab initio calculation indicates that the $O-H\cdots\pi$ interaction is energetically more favorable than the $C_{(AC)}-H\cdots O$ interaction. Experimentally, they located three minima with a cyclic geometry containing two hydrogen bond interactions. In the global minima, the main interaction was $O-H\cdots\pi$ with a the secondary interaction involving $C_{(AC)}-H\cdots O=C_{(FA)}$ with the carbonyl oxygen being the electron donor.

Sander et al. [12] also carried out microsolvation studies by employing matrix isolation infrared and ab initio calculations. As the simplest carboxylic acid, formic acid is a prototype for investigating hydrogen bond interactions of acids in solvents to understand the microsolvation. They studied the formic acid-water complexes and confirmed three minima corresponding to $HCOOH\cdots H_2O$ complexes with two hydrogen bonding interaction ($OH\cdots O$).

Rasanen et al. [13] performed studies of the formic acid dimer. Formic acid has multiple hydrogen bonding sites acting both as a donor and acceptor. Moreover, it also has syn as well as anti conformer. The anti conformer is lower in energy by 1365 cm^{-1} (3.66 kcal/mol). They found eleven dimers in inert gas matrixes, six anti-anti and five syn-anti dimers.

In order to address the hydrogen bonding behavior of multifunctional molecules, extensive research has been done on phenylacetylene [15,16] in association with different precursors. The diversity of intermolecular structures formed by phenylacetylene with various reagents is remarkable. The deprotonation enthalpy of the acetylenic group in phenylacetylene (1551 kJ/mol) is slightly lower than that of the acetylene (1590 KJ/mol). It indicates that the probability to form a $C-H\cdots X$ hydrogen bond should be marginally higher for phenylacetylene than for acetylene [14]. Based on the fact that water forms a $C-H\cdots O$ hydrogen bonded complexes with acetylene and water forms an $O-H\cdots\pi$ complexes with benzene, Patwari and his coworkers [15] studied phenylacetylene-water complexes. Unlike acetylene-water complex, the C-H stretching frequency shift was

marginal and furthermore the water molecule interacts with the acetylene moiety of the phenylacetylene submolecule, which was indicated by the disappearance of the Fermi resonance band corresponding to vibrations of the acetylenic moiety. This study suggests that the structure of phenylacetylene-water complex is surprisingly different from both benzene-water and acetylene-water.

Recently, π - π stacking as a weak interaction has also fascinated researchers. Patwari et al. [17] studied the π -stacked phenylacetylene dimer using IR-UV double resonance spectroscopy in combination with high level ab initio calculation. They located six different conformers of phenylacetylene dimers in which anti-parallel π -stacked structure appeared to be the most stable isomer.

1.5 Motivation for the present work:

At present, hydrogen bonding between simple donor and acceptor has been extensively studied whereas the molecules with multiple hydrogen bonding sites still remains a challenging problem. The multiple binding sites of a molecule provide the opportunity to investigate competitive hydrogen bonding. They can act as a proton donor or acceptor depending on the second molecular species, it interacts with, and environment. Usually, the multiple hydrogen bonding sites throws up a competition between electrostatic and dispersion energy terms in order to maximize the interaction energy. Molecules with multiple hydrogen bonding sites form several closely spaced minima on the potential energy surface of a dimer, which pose a challenge to study them experimentally.

In the present study, phenylacetylene and formic acid are chosen, since they provide multiple hydrogen bonding platforms. The active bonding sites are shown in **Figure 1**.

In phenylacetylene, both phenyl and acetylene π -clouds (Site A, Site B) can act as proton acceptor sites, whereas the acetylenic hydrogen (Site C) can act as proton donor. In formic acid, both the oxygens (Site E, Site F) carbonyl as well as hydroxyl, can act as proton acceptors and both the hydrogens (Site D, Site G) can act as proton donors. These multiple sites offered by the precursors can be expected to lead to several minima.

Matrix isolation spectroscopy provides an excellent method to study the hydrogen bonded systems with multiple bonding sites as described above, as it is known to trap local minima, in addition to the global minimum.

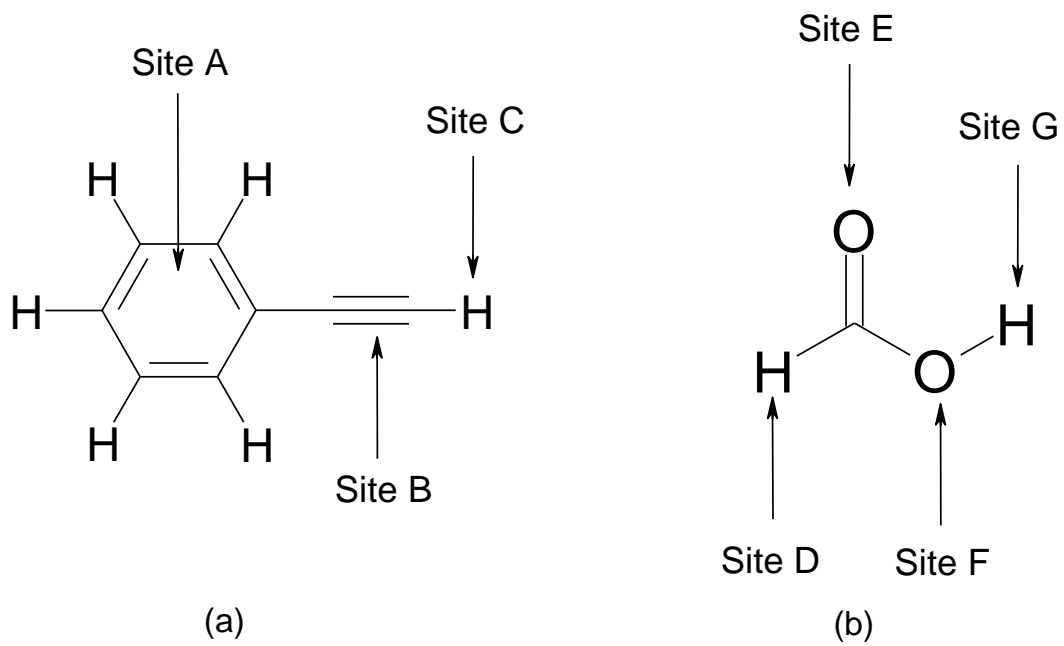


Figure 1- Structure of (a) Phenylacetylene, (b) Formic acid indicating the hydrogen bonding sites

1.6 Scope and objective of the present work:

In phenylacetylene, the leading interaction can switch from electrostatic to dispersion, which is already observed in literature while studying phenylacetylene-water and phenylacetylene-methanol complexes [16]. The dynamic behavior of the hydrogen bonding pattern in phenylacetylene can be expected to pose challenges in the experimental observation of the various minima. This thesis will provide a report on the study of the possible interactions between phenylacetylene and formic acid. Different computational methods have been used to find out possible adducts between the two monomers phenylacetylene and formic acid. To study the adducts experimentally, matrix isolation infrared spectroscopy has been set up. The complexes will be studied experimentally using the above facility for a corroboration between experiment and computations.

Chapter 2

Experimental and Computational Procedures

The present section deals with the experimental aspects of matrix isolation infrared spectroscopy and the computational methods which have been used to study the hydrogen bonded complexes of phenylacetylene-formic acid. The matrix isolation technique has been set up and this chapter discusses the instrumentation aspects of this experimental technique.

2.1 Matrix Isolation Technique

Matrix isolation spectroscopy is a technique where the analyte molecules are trapped in a large excess of an inert gas at very low temperature ($\sim 12\text{K}$). The species of interest are isolated in the rigid gas matrix and hence the term *matrix isolation*. To achieve isolation, typical matrix to sample ratios used are from $10^3:1$ to $10^5:1$. The trapped species may be stable molecules or transient species, such as ions or radicals.

This technique was initially proposed and developed by George C. Pimentel and his coworkers in mid 1950s, to study the free radicals [18]. Reactive species trapped in inert gas matrixes have long lifetime for want of reaction partners and hence can be easily studied by spectroscopic techniques such as infrared, UV-Visible, microwave, electron spin resonance spectroscopy. Although this technique was developed for the study of reactive species, it offered the additional advantage of small linewidths, which is described later in this chapter, and which has made this technique a powerful tool to study the weakly bound complexes and conformations of molecules.

Generally in the matrix isolation technique, inert gases and nitrogen are used as the matrix gases because of their inertness. In addition to chemical inertness, there are several properties the material should satisfy, to be a useful matrix material. Some of the important properties are low volatility at the temperature of study of interest, optical transparency in the region of interest, low latent heat of fusion and acceptable thermal conductivity.

2.2 Advantages:

In the matrix isolation technique, the molecules are isolated in a solid inert matrix, and hence do not experience intermolecular interactions. Furthermore, collision and Doppler broadening are absent since the molecules are immobilized in the frozen matrix. The trapping of molecule at very low temperatures ensures that only the lowest electronic and vibrational levels are populated. For all the above reasons, the matrix isolated spectra are generally simple and sharp, unlike vapour phase or condensed phase spectra, which show relatively large linewidths and spectral congestion.

2.3 Matrix environmental effects:

Even though the matrix is considered inert, in reality, the matrix often perturbs the spectra of the trapped species, to a small extent, due to a variety of reasons. The matrix effects are manifested through the modification of vibrational band shapes, intensities and frequencies, and in some cases cause a single vibrational mode to have a multiplet structure. These effects are discussed below.

2.3.1. Multiple trapping sites

The guest species are generally trapped either in substitutional sites or in interstitial holes in the matrix. The weak intermolecular forces existing between the matrix and the guest species will be different in the different sites. It is therefore possible that different types of matrix cages may induce different shifts leading to broadening or splitting of bands. The intensity of each band corresponding to the different sites varies according to the stability of the trapping sites. Annealing of the matrix at elevated temperatures (~35K) causes the unstable sites to vanish, thus generally sharpening the spectral features. The bands arising from the molecules trapped in a stable site, however, persist even on annealing. Varying the rate of deposition can also alter the distribution of the different sites, and this effect can be used to study the problem of unstable sites. Isolating the molecules in a different matrix also helps in the identification of bands due to splitting, since it is unlikely that two different matrices will give rise to similar trapping sites.

Degenerate vibrational bands can also be split in the matrix, if the cage in which the guest molecules are trapped presents a site of low symmetry lifting the degeneracy of the vibrational band in question.

2.3.2 Molecular Rotation

In the rigid, frozen matrix, free rotations are inhibited, since the molecules are tightly held and are immobilized. It is reported that for small molecules [19] such as ammonia, water, alkali halides, methane, quantized rotation may be possible in some matrices. For example, evidence has been presented that ammonia and water molecules rotate in an argon matrix but not in a nitrogen matrix [20]. The rotational features are identified by reversible intensity changes on temperature cycling, as opposed to splitting due to matrix site effects which are not reversible on temperature cycling.

2.3.3 Aggregation

Matrix isolation experiments are performed using typical matrix to solute ratios of 1000:1, at which ratios molecular isolation is reasonably assured. As the solute concentration in the matrix increased, molecular aggregates such as dimers, trimers and multimers may be produced in addition to the monomers. The feature due to aggregation or self-association are generally identified, by performing concentration dependence and warm-up experiments in which monomers diffuse to form dimers and higher multimers. Modification in vibrational band can also be observed if two species are trapped very nearby resulting in overlap of their respective cages. We can calculate the probability to ensure the maximal isolation of the analyte molecules. For example, take a carbon monoxide molecule, which occupies a single substitutional site, the probability of intermolecular interaction is simply the chance of finding another molecule occupying one of the 12 sites that form the cage. The chance for absence of second CO molecule is given by the formula $P = (1-r)^{12}$, where r is the reciprocal of the matrix ratio. For very small value of r the expression becomes $P = (1-12r)$, from this it is clear that the matrix ratio of 1000 is needed to ensure 99% isolation.

2.3.4 Matrix shifts

The solute molecules trapped in a matrix under conditions of perfect isolation, experience weak solute-matrix interactions. These interactions can result either in a shift in the frequency or splitting of the bands. The frequency shift, $\Delta \nu$ in a matrix with respect to the gas phase value arises from electrostatic ($\Delta \nu_{elec}$), inductive ($\Delta \nu_{ind}$), dispersive ($\Delta \nu_{dis}$) and repulsive interactions ($\Delta \nu_{rep}$) and is given by the expression [19],

$$\Delta \nu = (\nu_{matrix} - \nu_{gas}) = \Delta \nu_{elec} + \Delta \nu_{ind} + \Delta \nu_{dis} + \Delta \nu_{rep} \dots\dots\dots(2.1)$$

where ν_{matrix} and ν_{gas} are the frequencies of the vibrational mode of a molecule in the

matrix and gas phase respectively.

In rare gas and in nitrogen, these shifts are usually small and electrostatic interaction is absent. In inert gas matrices, the long range London dispersion forces and the short range repulsive forces are the two dominant interactions. A theoretical treatment of a matrix induced frequency shift has been given by Pimentel and Charles [21]. It has been shown that a tight cage usually introduces a blue shift in the vibrational frequencies (relative to the gas phase values) and a loose cage a red shift.

The frequency shift, $\Delta \nu$, in solutions arising from the perturbation due to solvent interactions is given by the Buckingham expression [22],

$$\Delta \nu = (\nu_{\text{solvent}} - \nu_{\text{gas}}) = [B_e/hc\omega_e] [U'' - 3AU'/\omega_e] \dots \dots \dots (2.2)$$

Where, $B_e = h/8\pi^2\mu cr_e^2$, is the rotational constant,

A is the anharmonicity constant,

$$U' = \{\delta U/\delta r_{bc}\} \quad \text{and} \quad U'' = \{\delta^2 U/\delta r_{bc}^2\}$$

$c\omega_e$ is the harmonic oscillator frequency for the normal vibration, Q.

This expression can be used to explain the frequency shift occurring in the matrix. **Figure 2** shows the potential curves for a polyatomic molecule trapped in a matrix cage. When R_{CM} is greater than R_1 , i.e., when one of the atoms, C, of the trapped molecule is more distant from the matrix atom, M, U' and U'' are negative, the term $\Delta \nu$ is negative (Eq. 2.2). When R_{CM} is less than R_e (equilibrium distance), U' and U'' are positive and hence $\Delta \nu$ is positive. When R_{CM} is less than R_e , the molecule experiences a tight cage effect, which induces a positive frequency shift (i.e. blue shift). When R_{CM} is greater than R_1 the molecules experience a loose cage effect inducing a negative frequency shift (red shift). It was reported that when polyatomic molecules are trapped in matrices, the high frequency stretching, bending or rocking vibrations, give positive shifts as in a tight cage [21].

2.4 Characteristics of matrix materials

The most commonly used matrix materials are inert gases (except He) and nitrogen. Depending on the type of experiment and the cryostat available, one can choose a matrix gas. A temperature of at least 20 K is required for N_2 , Ar, Kr and Xe, but Ne requires a temperature less than 9K. Hydrocarbons are considered as good matrices in the UV region, because scattering is less for glassy matrix than for a crystalline matrix. While choosing a matrix, following properties have to be considered.

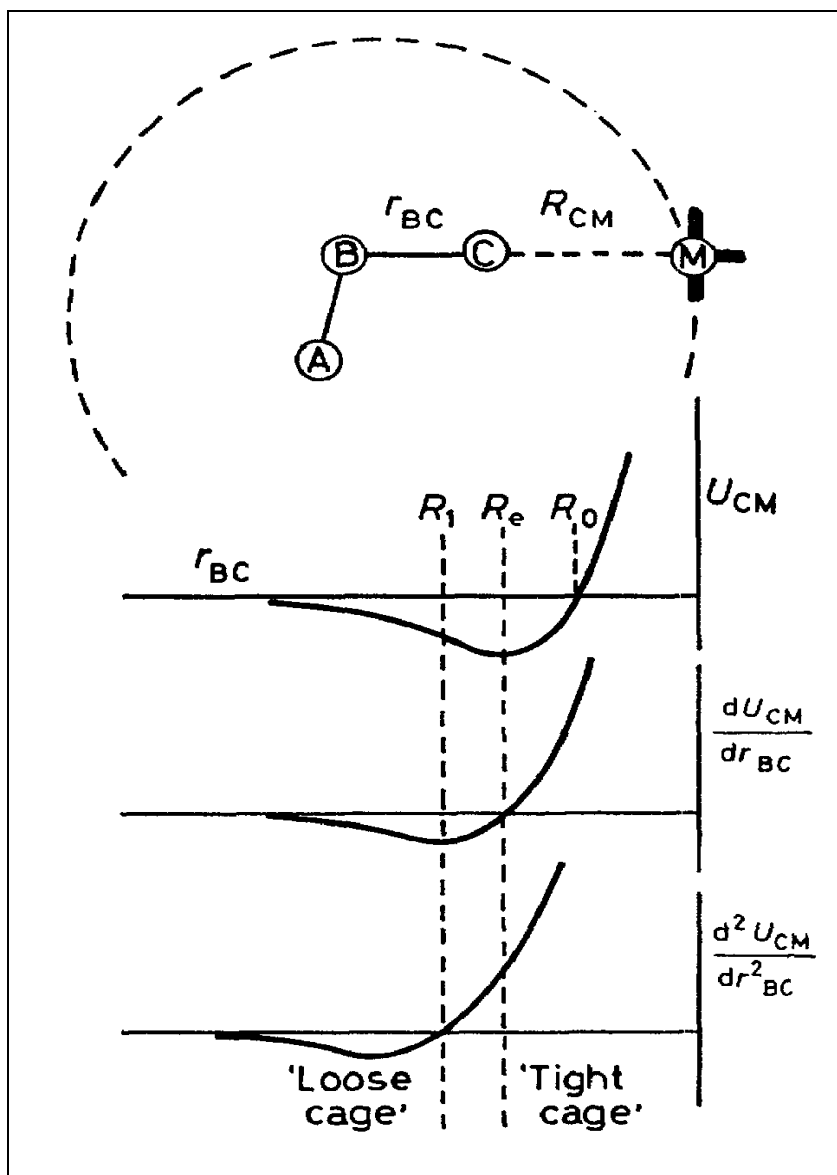


Figure 2 - Potential energy curves for a polyatomic molecule trapped in a matrix [19].

2.4.1 Inertness

In order to minimize the matrix-sample interaction, the matrix must be inert in nature. Among the noble gases, the reactivity increases as we go down the group, because of the increase in polarizability [23]. This is one of the reasons why argon is chosen as the matrix gas among the rare gas.

2.4.2 Rigidity

Rigidity of the matrix influences the diffusion of the trapped species, which is a temperature dependent property. The temperature of the matrix should not exceed about one third of the melting point of the solid matrix. The upper limit of the required temperatures are 9 K for Ne, 29 K for Ar, 40 K for Kr, 55 K for Xe and 26 K for N₂ [20].

2.4.3 Transparency

Noble gases and nitrogen are transparent in IR and UV visible regions. The matrix should be absorption-free in the spectral regions of interest; otherwise overlapping of matrix bands may lead to erroneous spectral interpretation. Light scattering is also an important factor to be considered. The temperature and the rate of deposition used to prepare the matrix, decide the quality of the matrix and hence the scattering and the transparency of the matrix. Rapid deposition rate leads to peeling of the matrix. Deposition at low temperature enhances the isolation but the scattering of light is more at lower temperatures because of the absence of the perfect crystal structures.

2.4.4 Volatility

The matrix must have enough vapour pressure at room temperature for the proper mixing with the sample species. However, at cryogenic temperatures, its vapour pressure should be low so that it can form a rigid and stable matrix.

2.4.5 Latent heat of Fusion and thermal conductivity

Though the latent heat of fusion (L_f) and thermal conductivity (λ) of the matrix do not affect the guest diffusion during condensation, rate of deposition has to be controlled to avoid temperature rise. Moskovits and Ozin [24] related the temperature rise with the rate of deposition and time of deposition using an expression

$$T = (T_0 + L_f n^2 t) / \lambda \rho A^2$$

Where T and T_0 are the surface and interior temperatures of the matrix layer,

n = rate of deposition

t = time of deposition

ρ = molar density of the matrix

A = surface area

The expression shows that temperature rises as the square of the deposition rate and linearly with time.

2.5 Matrix Structure

The noble gases, except helium, crystallize in face-centered cubic lattices. Nitrogen below 35 K and CO below 62 K also crystallize in FCC structure [25]. In an FCC crystal a species is most likely to be trapped in a substitutional site where a guest molecule replaces a host molecule. The guest species in a trapped site is surrounded by 12 nearest matrix atoms. The accommodation of a molecule of reasonable size in a vacant site created by the removal of one matrix atom is not possible. Hence, most species will occupy a 'cage' consisting of more than one substitutional site. Removal of two matrix atom gives rise to a site with 18 nearest matrix atoms [20]. The substitutional site formed by the removal of three matrix atoms in a triangle will make a site with 22 nearest neighbours and the loss of three atoms in a row will give rise to 24 nearest neighbours.

In addition to the substitutional site, the crystal lattice can also have interstitial sites, a tetrahedral site (T) and an octahedral site (O). A tetrahedral site has four nearby host atoms, one sphere resting upon the three other touching spheres. An octahedral site is formed by the arrangement of six adjacent host atoms. Only species of small sizes can be accommodated in an octahedral site. It is unlikely that tetrahedral site can be occupied without serious lattice distortion [25]. A guest molecule with a spherical diameter of 0.159 Å and 0.293 Å can be accommodated in a tetrahedral and an octahedral site respectively.

2.6 Equipment

The main components of the matrix isolation setup involve a cryostat, vacuum system and an FTIR spectrometer, which are described separately. The photograph of matrix isolation IR spectroscopy of our lab and its main components are shown in the **Figure 3** and **4**.

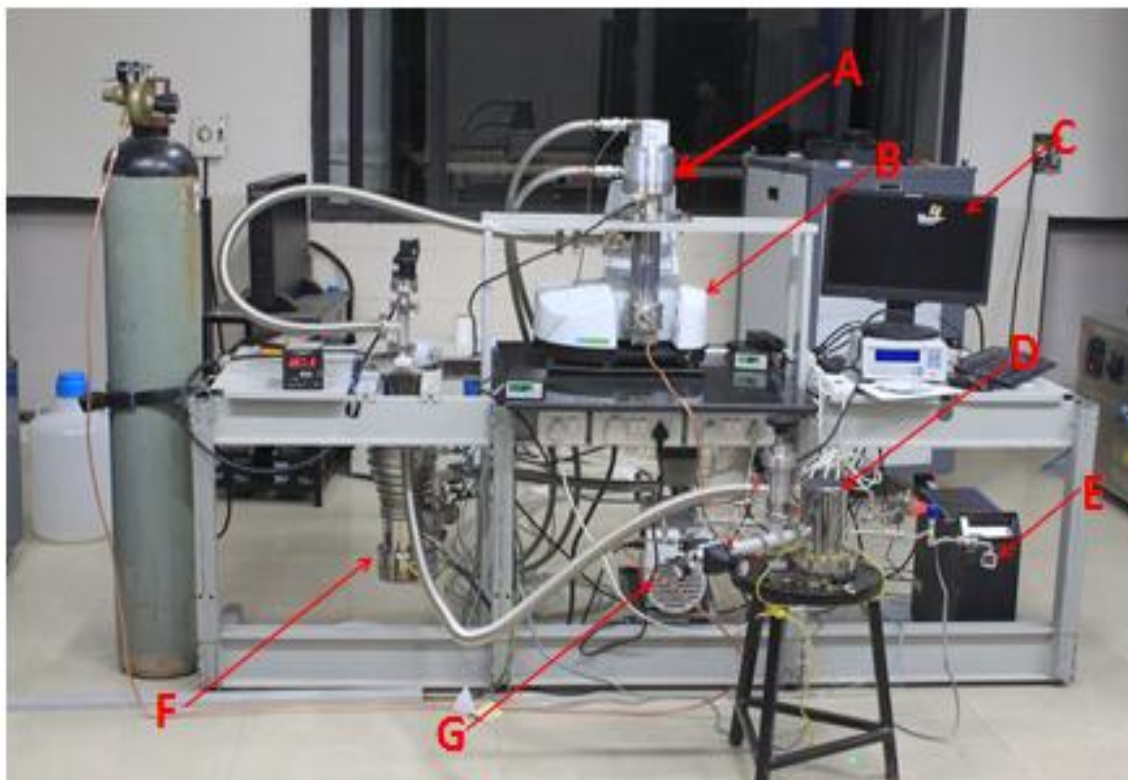


Figure 3 - Photograph of the Matrix Isolation IR spectroscopy set-up.

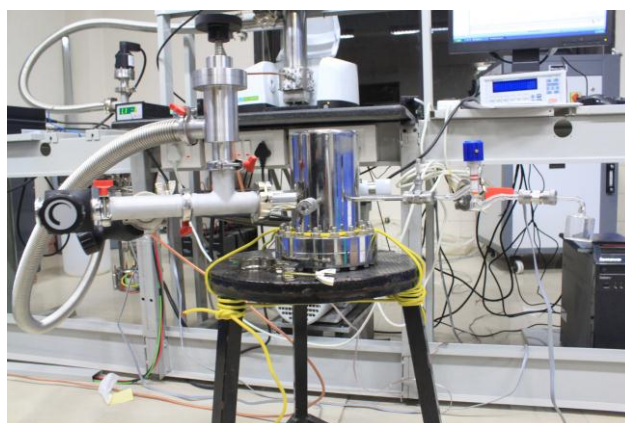
(A) Cryostat; (B) FTIR spectrometer; (C) Data acquisition system; (D) Mixing Chamber; (E) Sample Container; (F) Diffusion pump; (G) Rotary pump.



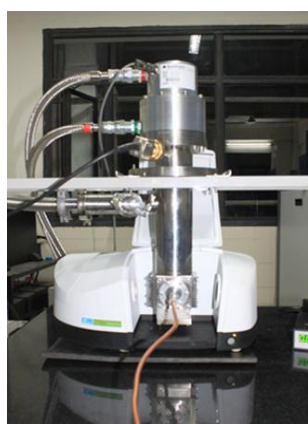
A .Cryostat



B .Diffusion Pump



C. Mixing chamber with sample container



D. FTIR Spectrometer



E. Temperature Controller

Figure 4 - Main Components of Matrix Isolation IR spectroscopy set up

2.6.1 Cryostat based on a closed cycle helium Compressor

The set-up that has been built utilizes a Sumitomo closed cycle helium compressor cooled cryostat (HC-4E1 Helium Compressor). The four main parts of the cryostat are: A) cold head B) a helium compressor, C) a temperature control unit and D) an optical extension set.

A&B) Cold Head and Compressor:

The basic unit of the closed cycle cryostat is a cold head, also referred as expander in the Gifford-McMahon refrigeration cycle. It is connected to a compressor by two gas lines and an electrical power cable. One of the gas lines supplies high pressure helium gas to the expander, the other gas line returns low pressure helium gas from the expander. The compressor (Sumitomo cryogenics, Model No: HC-4E1) provides the necessary helium gas flow rate at the high pressure for the expander to convert into the desired refrigeration capacity. The heat generated due to compression of the gas of compressor and diffusion pump was removed by a 3 KW chiller. The photograph of compressor and chiller is shown below in **Figure 5**.

Working principle:

The close cycle cryostat operates on the principle of Gifford-McMahon refrigeration cycle, often shortened to GM cycle. The pneumatically driven GM cycle is different from mechanically driven GM cycle where an internal pressure differential is used to move the displacer instead of a mechanical piston, resulting in reduced vibrations. The refrigeration cycle of the closed cycle cryostat starts with the rotation of the valve disk opening the high pressure path allowing the high pressure helium gas to pass through the regenerating material into the expansion space. Second, the pressure differential drives the displacer allowing the gas at the bottom to expand and cool, which provides the low temperature at the cold head. Third, the rotation of the valve disk opens the low pressure path allowing the cold gas to flow through the regenerating material removing heat from the system. Finally the pressure differential returns the displacer to its original position completing the cycle. The schematic of the cryostat has been shown in **Figure 6 (a), (b) and (c)** [26]. The lowest temperature achieved by helium gas in Gifford-McMahon cycle is around 10 K.

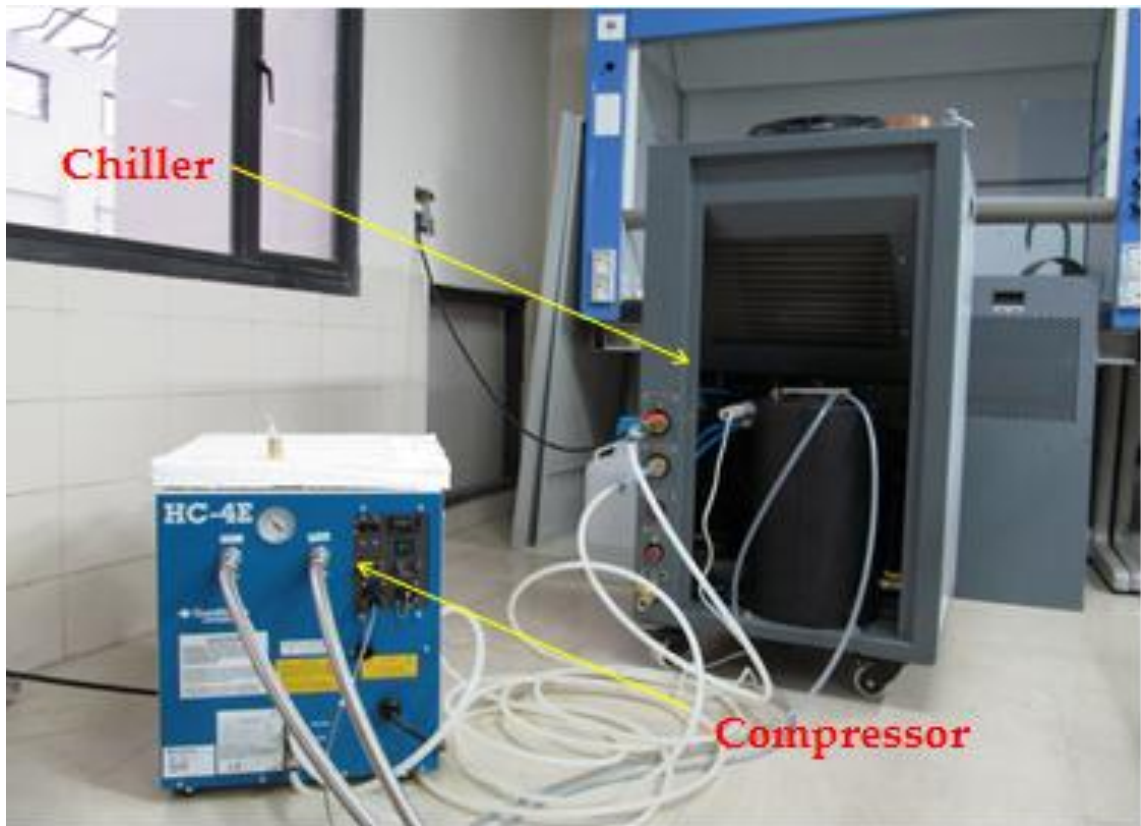


Figure 5 – Photograph of Compressor and Chiller

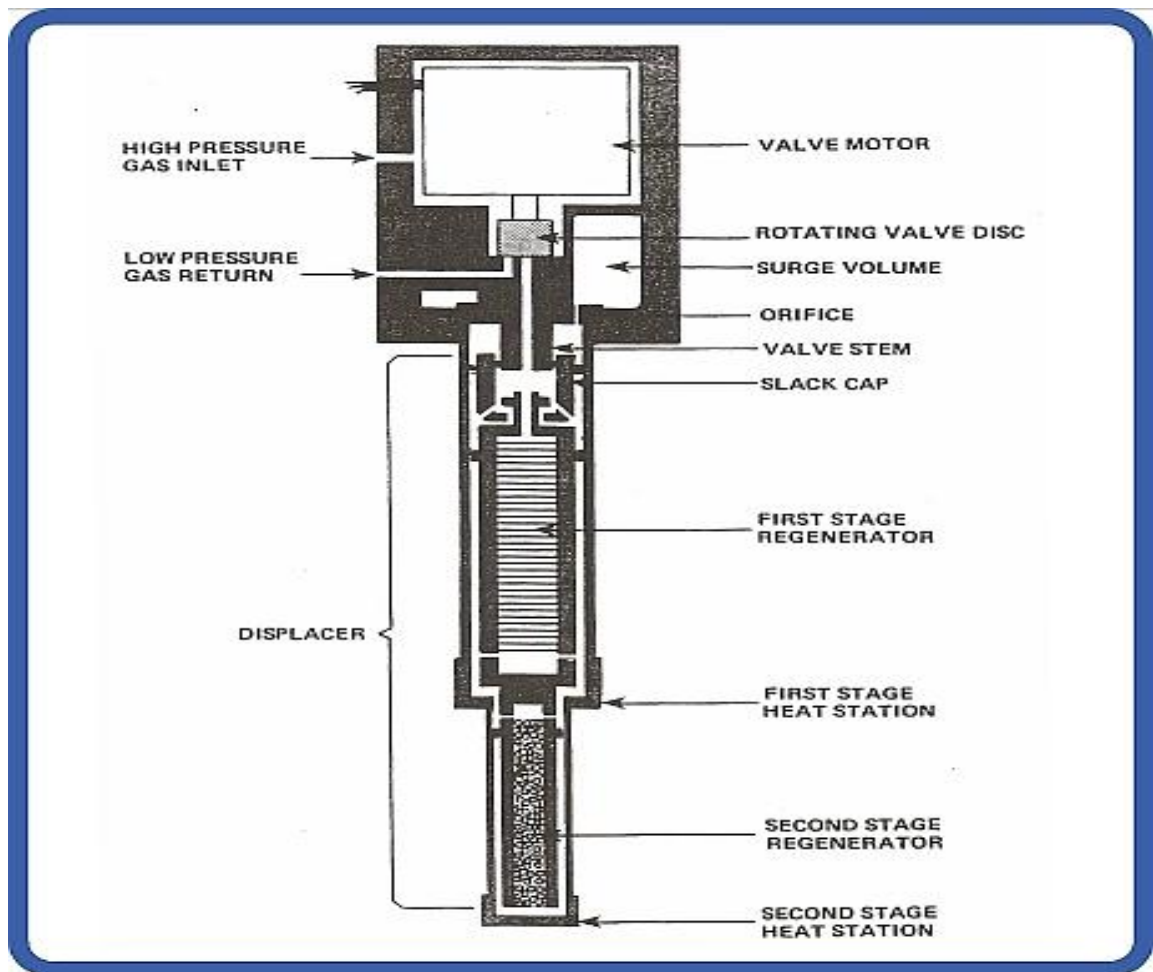


Figure 6 (a) - Block diagram of the internal structure

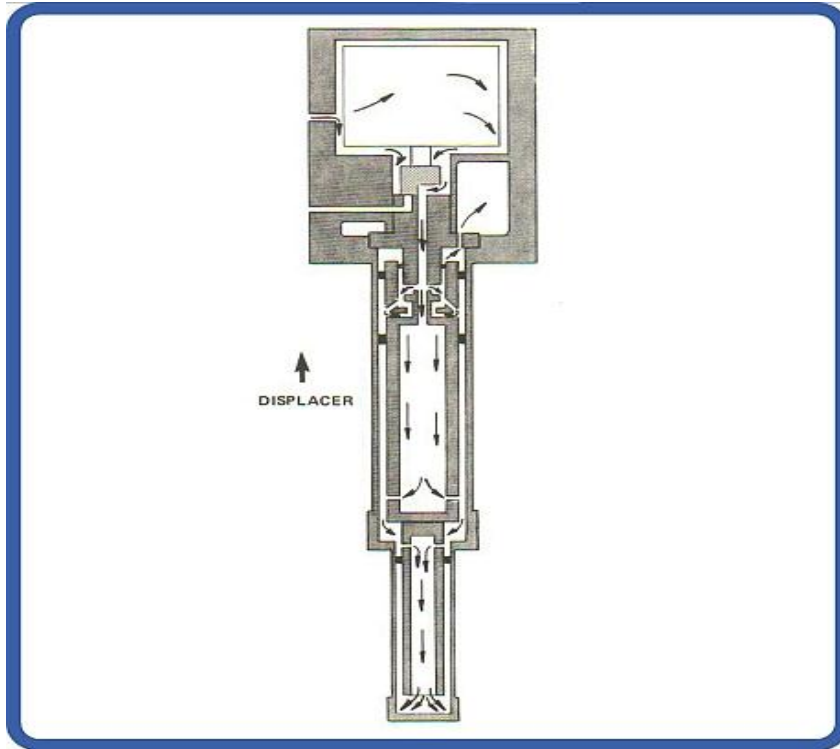


Figure 6 (b) - Steps 1 and 2 of the GM cycle

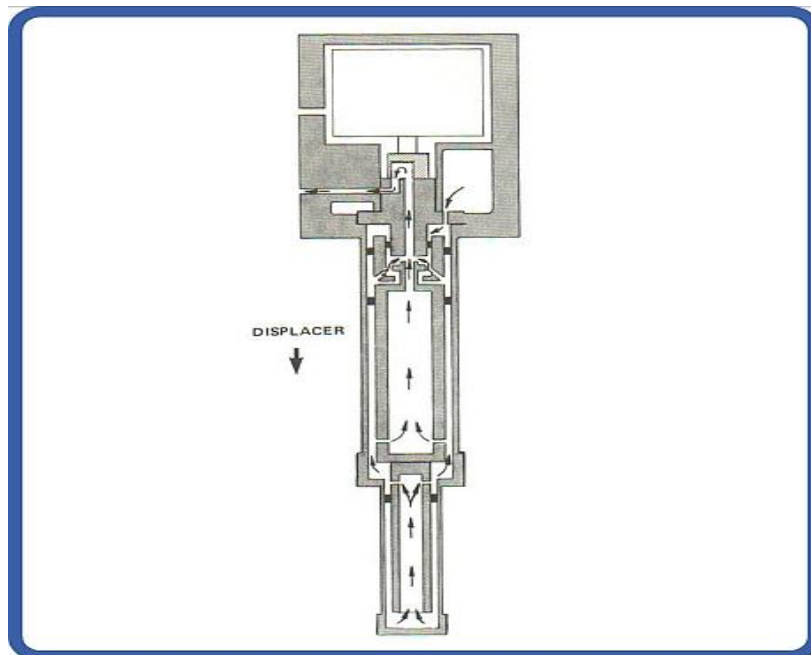


Figure 6 (c) - Steps 3 and 4 of the GM cycle

C) Temperature Control unit:

Temperatures above 12 K can be obtained using a heater coil mounted on the cold tip. The current through the heater is regulated using the temperature controller unit (Lakeshore 335 with PID controller). With this arrangement, the temperature can be varied from 12 K to 300 K. It is necessary to obtain temperatures above 12 K to anneal the matrix, which enhances the diffusion and promotes the reaction of the trapped species. Annealing is also done to examine the presence of multiple sites arising from unstable matrix sites.

Temperature measurements: The four thermometric methods that are generally employed to measure the low temperature are a) thermocouples b) solid state thermometers c) capacitance cryogenic temperature sensors d) hydrogen vapour pressure thermometers. In our cryostat, the temperature is measured with the help of silicon diode sensor.

D) The Optical extension unit:

The extension unit comprises of a substrate holder, a radiation shield and a vacuum jackets. The substrate holder is attached to the cold head of the cryostat, which attains a temperature of 12 K. A KBr substrate of 25 mm diameter and 4 mm thickness was mounted on the substrate holder. Radiation shield made up of copper is fixed around the cryotip. The rotatable vacuum jacket has four ports which is attached to another vacuum jacket through 'O' ring seal. KBr windows of 40 mm diameter and 4 mm thickness were mounted on two of the opposite ports of the rotatable vacuum jacket. These windows transmit the infrared beam to the detector. The third port is fitted with a quartz window for viewing purposes and when required to transmit UV-visible light to study the effect of photo irradiation on the matrix isolated sample. To the fourth port, a sample inlet system is connected, through which deposition is conducted.

2.6.2 Vacuum system:

The cryostat was evacuated by an oil diffusion pump (Edwards, Diffstack MK2 series 100/300) with a pumping speed of 280 litre/sec, backed by a rotary pump (Edwards). A second rotary pump (Hind Hivac, Model No: ED6) was used as a roughing pump for the vacuum system. Both rotary pumps have a pumping speed of 100 litre/min. A butterfly valve was used to isolate the cryostat from the diffusion pump. The base vacuum in the system was $\sim 10^{-6}$ mbar, which was measured using a cold cathode gauge (Model No: MKS 943). The pressure above 10^{-3} mbar was measured using a Pirani gauge

(Edwards APG 100 Active Pirani Gauge).

2.6.3 FTIR spectrometer:

We have used a Perkin Elmer FTIR spectrometer for our experiments. The theory and instrumentation of FTIR has been described in several literatures [27]. The resolution of the FTIR was set at 1 cm^{-1} for the recording the spectrum.

2.6.4 Sample Introduction system:

A mixture of analyte and matrix was prepared in a stainless steel mixing chamber of one liter capacity, which was connected to the cryostat through a single effusive nozzle. In some cases, where the samples have low vapour pressure, deposition can be carried out using a double jet nozzle system; through one nozzle, the matrix gas is allowed to effuse through, while the second nozzle was used to introduce the sample into the vacuum system.

2.7 Experimental procedure:

The sample bulb was thoroughly degassed prior to sample loading and was then loaded into the bulb. The samples were then subjected to several freeze-pump-thaw cycles before deposition. The samples were equilibrated at the required temperature, for about an hour, to obtain the desired vapor pressure over the sample. The temperature of the bath was measured using a platinum resistance thermometer. The desired matrix/sample ratios were thus obtained by controlling the vapour pressure over the sample. A stainless steel mixing chamber of one liter capacity was used to prepare matrix/sample gas mixtures. The mixture was then allowed to deposit on the cold KBr substrate through the nozzle system described above. Rate of deposition was controlled using a fine needle valve (Pfeiffer Vacuum, D-35614 Asslar).

2.8 Computational Procedure:

The computational study was carried out using the Gaussian 09 package [28] in Linux operating system. Molecular properties such as structures, energies and frequencies were calculated to corroborate our experimental results. AIM [29] package was used to examine the nature of the interactions between the precursors of the complexes. A brief discussion regarding the computations is given below.

There are many electron structure methods available for ab-initio calculations.

Some of the popular methods are: Hartree-Fock methods (HF), Density Functional Theory (DFT), Møller–Plesset perturbation theory (MP_n) (where n denotes the order of perturbation), Configuration interaction (CI), Coupled cluster (CC), Multi-configurational self-consistent field (MCSCF), Multi-reference configuration interaction (MRCI) etc.

DFT allows all electronic properties of system to be determined from the electron density which is a function of just three variables (x, y, z). One of such functional is BLYP (Becke-Lee-Yang-Parr) which includes some HF exchange. It involves both electron spin densities and their gradients. There are also hybrid functionals which define the exchange functionals as a linear combination of HF, local and gradient-corrected exchange terms. The most used such functional is B3LYP. The B3LYP method uses the Becke three-parameter non-local exchange functionals [30, 31] with non-local correlation of Lee et al. DFT includes electron correlation and hence more accurate than HF. Energy and orbital coefficients are solved by an iterative self-consistent field (SCF) method. It is an appropriate method for systems having upto 100 atoms. But recently, advance modifications in DFT functionals have been introduced, named as Minnesota functional (M06). It has been designed by employing some strategies. These are 1) constraint satisfaction, 2) modeling the exchange correlation hole, 3) empirical fits, and 4) mixing Hartree-Fock and approximate DFT exchange [32]. The M06 suites of functionals are set of four meta-hybrid GGA DFT functionals (generalized gradient approximation (GGA) in which the density functional depends on the up and down spin densities and their reduced gradient). The suite is believed to reproduce dispersion forces rather well. They are constructed with empirical fitting of their parameters but constraining to the uniform electron gas. The family includes the functionals M06-L, M06, M06-2X and M06-HF, with a different amount of exact exchange on each one. M06-L is fully local without HF exchange (not hybrid), M06 has 27% of HF exchange, M06-2X 54% and M06-HF 100%. The advantages and utilities of each one are [33]:

- M06-L: Fast, Good for transition metals, inorganic, and organometallics.
- M06: For inorganometallics, organometallics and non-covalent bonds.
- M06-2X: Main group thermochemistry, kinetics, noncovalent interactions, and electronic excitation energies to valence and Rydberg states
- M06-HF: Charge transfer TD-DFT, systems where self-interaction is extreme

Møller–Plesset perturbation theory of (MP) is a post Hartree-Fock (HF) ab-initio

methods. It improves on the HF method by adding electron correlation effect by means of Rayleigh-Schrodinger perturbation theory to second (MP2), third (MP3) and fourth order (MP4). Here, one considers an unperturbed Hamiltonian operator, and a small perturbation (often external) is added to it. Systematic studies of MP perturbation theory have shown that it is not necessarily a convergent theory at high orders.

2.8.1 Geometry optimization and frequency calculation:

A molecular structure corresponding to a minimum on the potential surface is obtained following a geometry optimization. A geometry optimization begins at the guess molecular structure specified as input, and steps along the potential energy surface. The energy and gradient are first computed at the point on the potential surface corresponding to the initial geometry. This information is used to determine how far and in which direction the next step is taken to improve the geometry. At the minimum or at the stationary point, the forces will be zero. In the case of Gaussian program, the optimization was achieved when the forces, the root mean square of forces, the calculated displacement and the root mean square of the displacement for the subsequent step are below the preset threshold values.

Optimization calculations were performed at various levels of theories using Hartree - Fock (HF), Moller-Plesset second order perturbation (MP2), Minnesota functions and Density functional methods (B3LYP) using a variety of basis sets. As mentioned above guess structures were used to start the optimization process, without imposing any symmetry constraints.

Vibrational frequency calculations were performed at the same level of theory used for geometry optimization. Analytical gradients were used in the computations, though in a few cases a numerical method was also used. Vibrational frequency computations were done, first to ensure that the computed structures did correspond to minima on the potential surface and also to assign the vibrational features observed in the experiments. The computed vibrational frequencies will be scaled for the purposes of comparison with experimental results. To arrive at the scaling factor the experimentally observed strongest feature will be correlated with the strongest feature indicated by the computations in the spectral region of interest. The scaling factor that will bring the computed frequency in good agreement with that of experiment will then be used to scale all other vibrational frequencies. The computed scaled frequencies will be used to simulate the vibrational spectra. The synthetic spectra were generated assuming a full

width at half maximum (FWHM) of 1 cm^{-1} , which is the typical resolution of our instrument. Zero point vibrational energies (ZPE) were also obtained from frequency calculations which were used to calculate ZPE corrected energies.

2.8.2 Stabilization energy calculation of complexes:

The stabilization energy of the complex was computed using the method described below. The stabilization energy (ΔE) of a complex is given by

$$\Delta E = E_{AB} - (E_A + E_B) \dots \dots \dots (1)$$

Where, E_A , E_B and E_{AB} represent the energies for the monomers A, B and complex AB respectively. If the value of ΔE is negative, the complex is more stable relative to the precursors. In further discussions, only the magnitude of ΔE will be given and imply the negative sign by the use of the term stabilization. The stabilization energy of the complex corrected for zero point energy (ZPE) was also calculated.

It has been observed that after the zero point correction, the stabilization energy becomes less negative. The zero point vibrational energy (ZPE) is equal to one half the sum of the vibrational fundamental frequencies. It can be easily seen that in the complex, there are six normal modes more than the sum of the normal modes of the two monomers. Assume that the two monomers of the complex have N_1 and N_2 of atoms respectively, in which case the complex will have (N_1+N_2) atoms. Assuming that both the precursors and the complex are non-linear molecules, the number of extra normal modes can be calculated as follows:

$$\text{Extra normal modes} = \{3(N_1+N_2)-6\} - \{(3N_1-6) + (3N_2-6)\} = 6$$

Therefore, the one half of the sum of vibrational frequencies of six extra normal modes is responsible to make stabilization energy less negative in the case of two monomers.

When the energy of complex (E_{AB}) is computed, the basis functions used are those of both the monomer subunits. Whereas, for computing the energy of the individual precursors (i.e. ΔE_A and E_B), the basis functions pertaining to only the corresponding precursors are used. As the number of basis functions used is larger in the computation of the complex, the energy obtained will be lower, as basically each monomer can use the basis functions of other. Stabilization energies thus derived from the calculated energies E_A , E_B and E_{AB} will be overestimated and the error is referred to as the basis set superposition error (BSSE). Although the origin of BSSE is well understood, there is no easy way to correct it. The best way to eliminate the BSSE is to increase the basis set

until the stabilization energy is stable to the desired accuracy, which of course implies large computation times for even small systems. The commonly used method to correct for BSSE is by counterpoise correction proposed by Boys and Bernadi [34]. In this scheme, one calculates all quantities (energies of monomer EA, EB and the complex EAB) in the same basis set spanned by the functions of the complex AB and the difference is obtained as follows.

$$\Delta E = E_{AB}(AB) - \{E_A(AB) + E_B(AB)\} \dots \dots \dots (2)$$

Where, $E_A(AB)$ = Energy of the monomer A using the basis set AB

$E_B(AB)$ = Energy of the monomer B using the basis set AB

$E_{AB}(AB)$ = Energy of the complex AB using the basis set AB

In our studies, the stabilization energies of the complex corrected for the BSSE have also been included. BSSE correction term is evaluated as follows:

$$\text{BSSE correction} = \{E_A(A) - E_A(AB)\} + \{E_B(B) - E_B(AB)\}$$

Here, $E_A(A)$ = Energy of the monomer A using the basis set A

$E_A(AB)$ = Energy of the monomer A using the basis set AB

Similarly, $E_B(B)$ and $E_B(AB)$ are also defined.

The BSSE correction term turns out to be positive. When this term is added to the raw stabilization energy, a negative quantity, the overall BSSE corrected energy becomes less negative.

Corrections of energies for ZPE and BSSE [34] simultaneously were not included as these values are known to overcorrect the stabilization values.

2.8.3 Atoms –in-molecules (AIM) methodology

Bader first proposed the atoms in molecules theory, which uses an analysis of the electron density topology [35]. The wave function corresponding to the optimized geometry of a molecule or complex is generated using the Gaussian-09 package. From the electron density plots, one obtains bond critical points, charge density (ρ), Laplacian of charge density ($\nabla^2\rho$), which is also the trace of Hessian of ρ . The charge density, $\rho(r)$, is a physical quantity which has a definite value at each point in space. It is a scalar field defined over three dimensional space. Each topological feature of $\rho(r)$, where it is a maximum, a minimum, or a saddle point, has associated with it in a space called a critical point, where the first derivative of $\rho(r)$ vanishes. The sign of its second derivative or curvature at this point determines whether a function is maximum or minimum. The topological properties of such a scalar field are conveniently summarized in terms of the

number and nature of its critical points. The rank of critical point, denoted by ω , is equal to the number of non-zero eigenvalues or non-zero curvature of ρ at the critical point. The signature denoted by σ , is the algebraic sum of the signs of the eigenvalues. The critical point (CP) is labeled by giving the values (ω, σ) . For example, (3,-1) critical point means, three non-zero curvatures and one positive and two negative eigenvalues. A (3, -1) CP correspond to a bond between two atoms, a (3, +1) CP to a ring, a (3, +3) CP to a cage and a (3, -3) CP corresponds to a maximum. The numbers of critical points of all types, which can coexist in a system with a finite number of nuclei, are governed by the Poincare- Hopf relationship,

$$n - b + r - c = 1$$

where, n is the number of nuclei, b is the number of bond critical points, r is the number of ring critical points and c is the number of cage critical points.

The sum of three Hessians ($\lambda_1, \lambda_2, \lambda_3$) at a bond critical point, the quantity $\nabla^2\rho$, provides a useful characterization of the manner in which the electronic charge density is distributed in the inter nuclear region. If the value of charge density ρ ($<10^{-1}$ au) and the curvature of charge density are large, Laplacian of charge density may be positive or negative usually in the same order of magnitude as ρ then the interaction is of shared type, typical of covalent interaction. For the closed shell interactions, such as hydrogen bond complexes, van der Waals complexes and ionic systems, the charge density ρ ($\sim 10^{-2}$ to 10^{-3} au) at the bond critical point is quite small and the Laplacian of the charge density is positive.

Chapter 3

Results and Discussions

3.1 Introduction:

Formic acid (FA) has two planar conformers that differ by the orientation of a hydrogen atom with respect to the C-O bond. The anti form is lower in energy than syn form by 3.66 kcal/mol [13]. Formic acid has four different hydrogen bonding sites, where both hydrogens, the O-H and the C-H, can serve as proton donors, while both oxygens as proton acceptors.

On the other hand, phenylacetylene (PhA) has two π -clouds which act as proton acceptors and the acetylenic hydrogen atom of phenylacetylene can serve as the hydrogen bond donor.

In order to investigate the competitive hydrogen bonding between molecules having multiple hydrogen bonding sites, we studied the complexes of phenylacetylene and formic acid.

3.2 Computational details:

The computational study was performed using the GAUSSIAN 09 program suite. The equilibrium geometries and vibrational frequencies were calculated using the density functional theory (DFT) using the Minnesota functionals M06-2X and B3LYP hybrid functional and second order Moller-Plesset perturbation theory (MP2) with a 6-311++G (d,p) basis set. The stabilization energies were calculated at each of these levels of theory, as follows:

$$\Delta E = E_{AB} - (E_A + E_B)$$
$$\Delta E_{BSSE} = E_{AB}(AB) - \{E_A(AB) + E_B(AB)\}$$

Stabilization energies were also individually corrected for the zero point energy (ZPE) and the basis set superposition errors (BSSE). BSSE correction was implemented using the counterpoise (CP) scheme of Boys and Bernadi [34]. The frequency calculations were performed at all the level of theories mentioned above to ensure that the optimized geometries were indeed a minimum on the potential surface and also to aid us in assigning the features observed in the experiments. Using the computed experimental

frequencies, the infrared spectrum of the complexes and the monomers were also simulated using Gauss-View assuming a linewidth of 1 cm^{-1} . Atoms in Molecule theory was performed to identify the critical points in the complexes to understand the bonding features.

As phenylacetylene and formic acid have multiple sites for hydrogen bonding interaction, and further given the fact that formic acid exists in two different conformations, multiple minima can be expected on the potential surface. While gas phase studies can only observe the global minimum, matrix isolation spectroscopy can locate local minima in addition to the global minimum and hence the motivation for the study of the complexes using matrix isolation spectroscopy.

3.4 Experimental details:

The matrix isolation facility has been successfully set-up in the lab. Since moisture cannot be eliminated completely from the system, mere deposition of the nitrogen matrix at 12 K yields the spectrum of matrix isolated water, which was done to check the working of the system.

In the spectrum of matrix isolated water (**Figure 7**), peaks at 3727 and 3634 cm^{-1} corresponding to antisymmetric and symmetric stretch of O-H, and a peak at 1597 cm^{-1} corresponding to bending mode of water were observed, consistent with literature reports. The small feature at 3715 and 1601 cm^{-1} is due to the formation of the H_2O dimer. The spectral features of water obtained in this experiment are in good agreement with reported values in literature [36].

3.3 Results and Discussions:

As described above three different methods M06-2X, MP2 and B3LYP were used for the calculation of the phenylacetylene-formic acid complex, using a 6-311++G** basis set. At each of the levels of theory indicated above, 14, 13 and 12 structures, respectively, were located corresponding to a minimum on the potential surface. The structures obtained at each of the above levels of theory are shown in **Table 2**.

The **Table 2** shows all the optimized geometries obtained on the various levels of calculations. They have been arranged in order of decreasing BSSE corrected stabilization energy, as calculated using the M06-2X level.

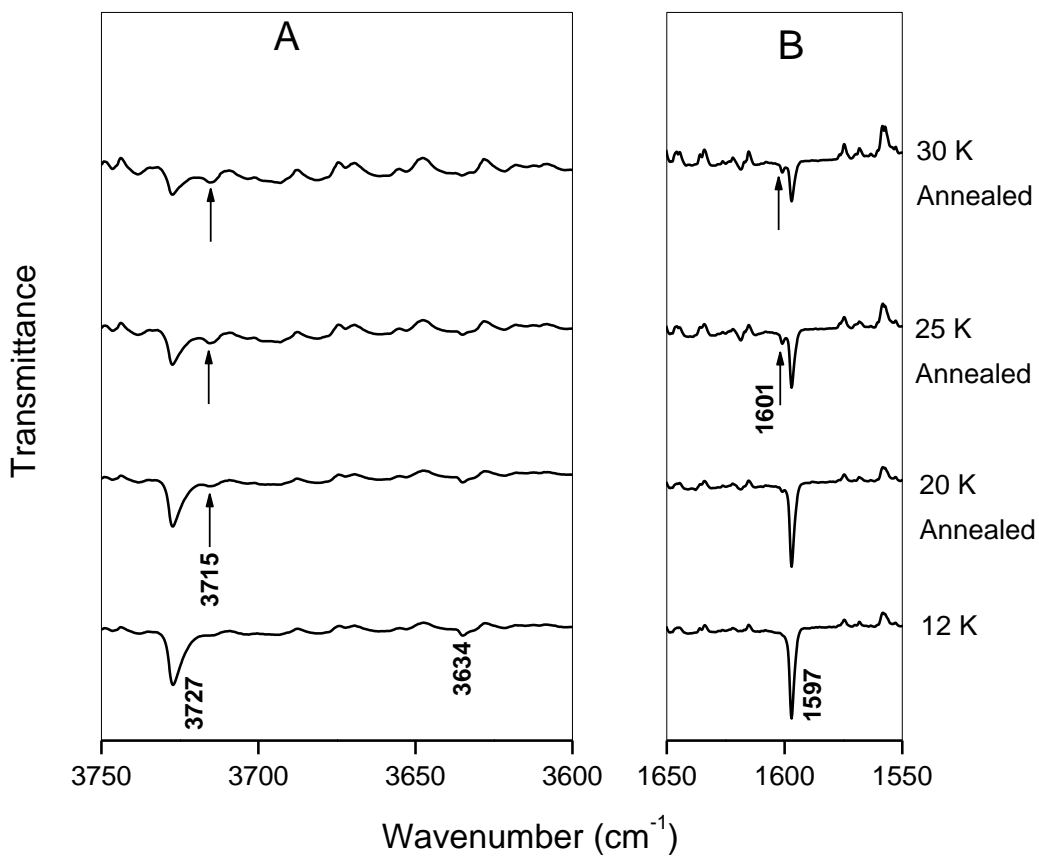
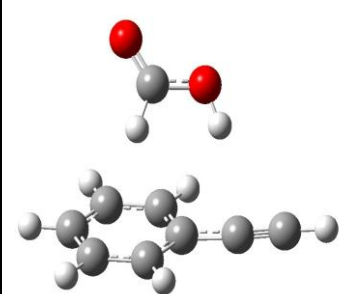
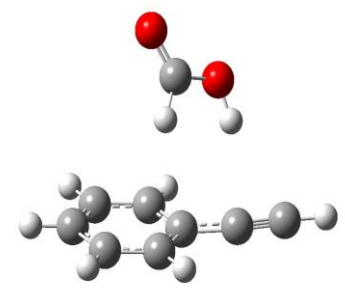
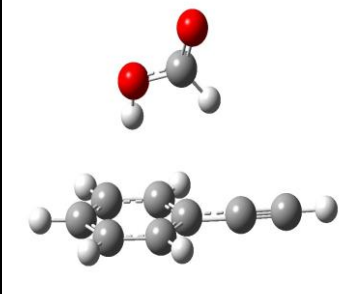
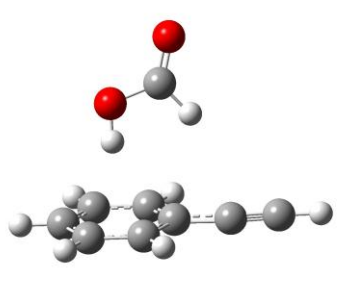
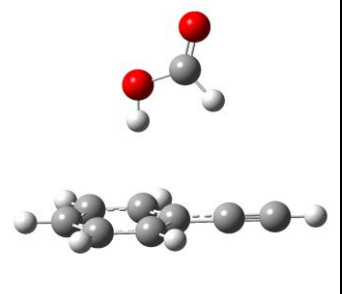
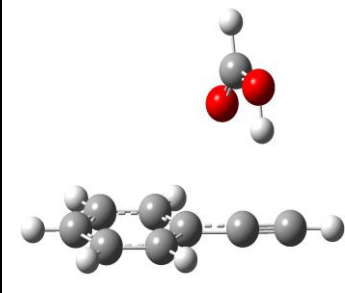
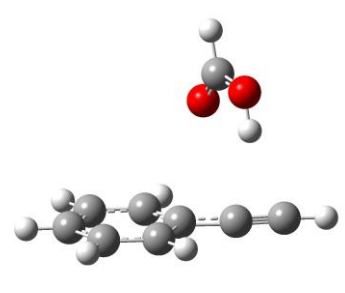
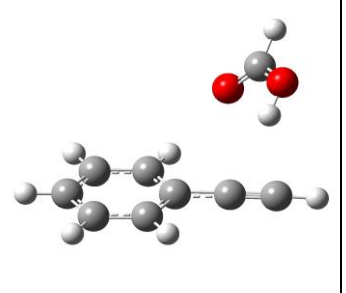
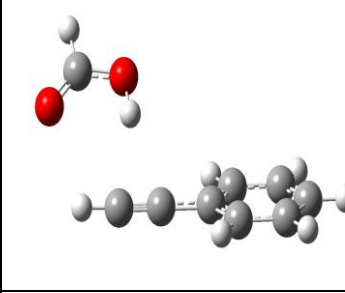
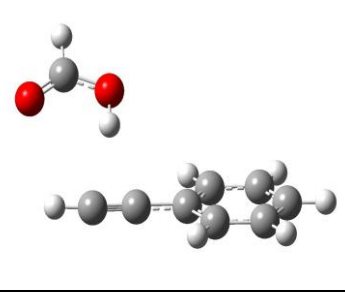
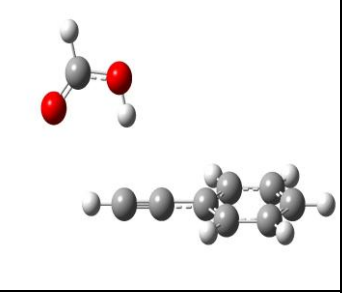
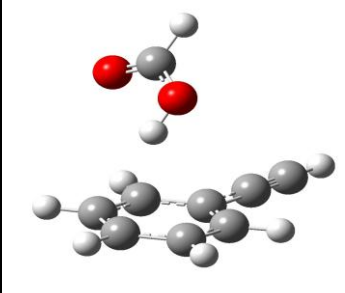
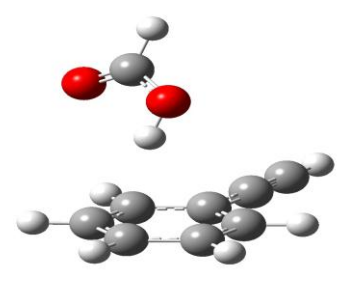
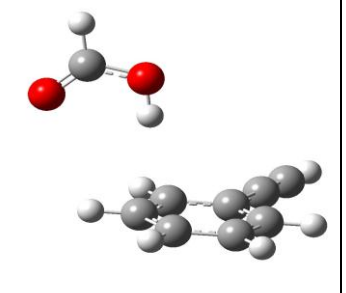
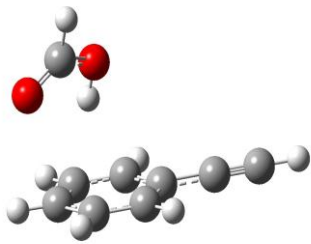
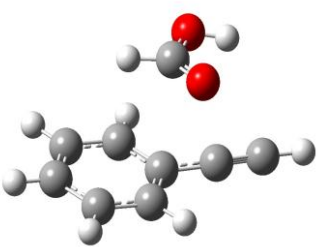
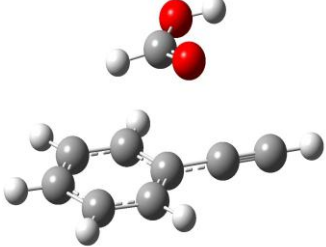
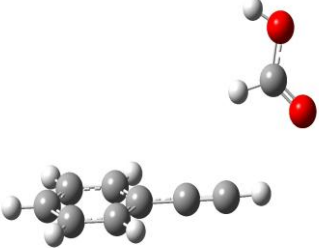
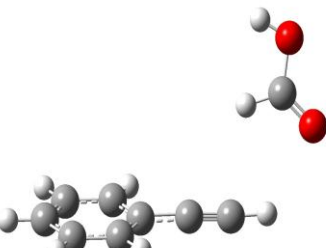
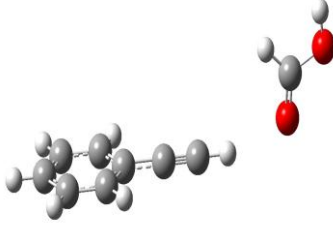
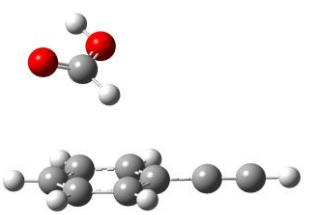
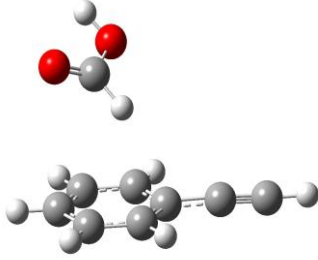
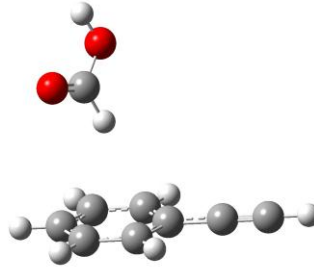
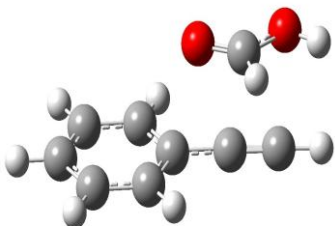
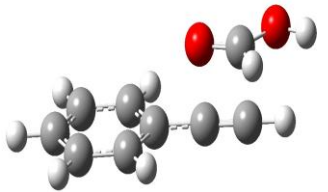
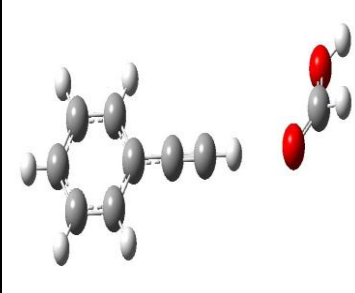
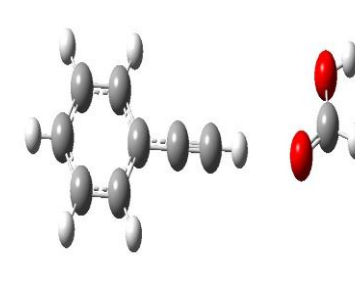
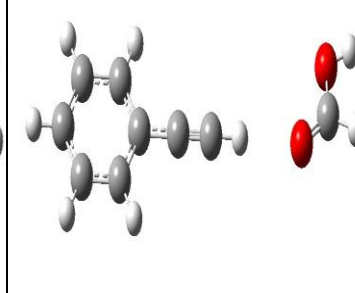
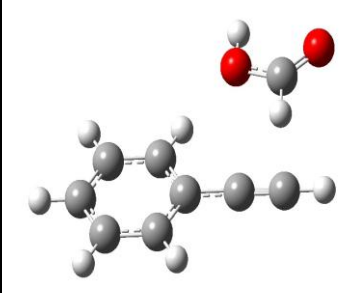
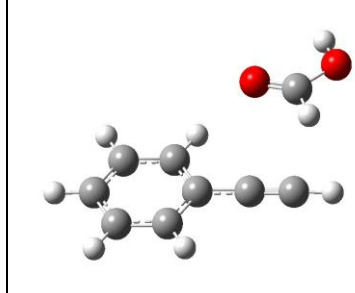
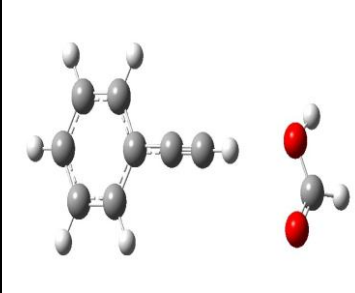
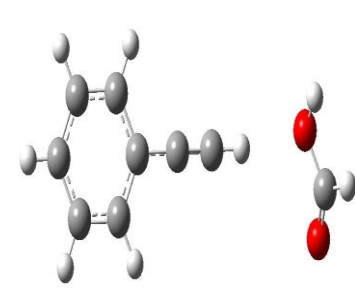
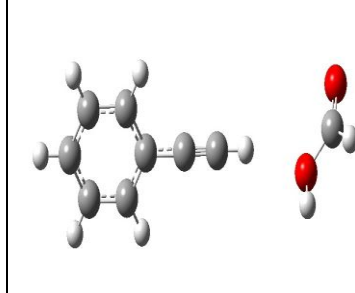
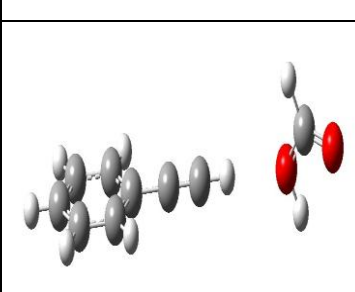
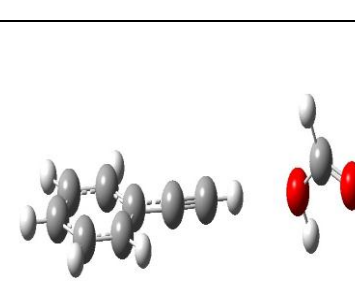
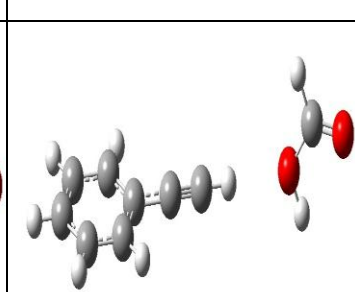
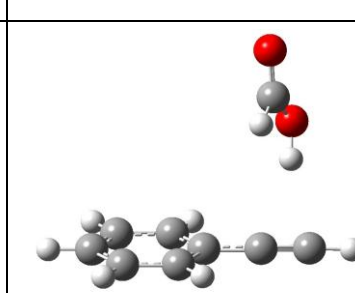
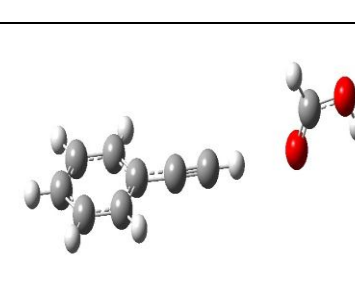
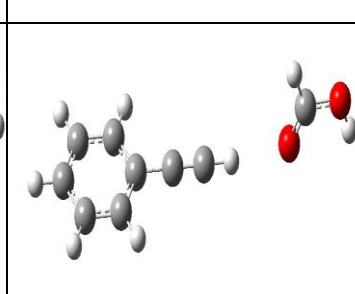


Figure 7 – IR spectra of water in N₂ matrix at 12 K. (a) water (sample maintained at 12 K); (b) Matrix annealed at 20 K for 10 minutes; (c) Matrix annealed at 25 K for 10 minutes; (d) Matrix annealed at 30 K for 10 minutes.

Table 2 - Optimized geometries of different complexes at different levels calculation

Complexes	M06	MP2	B3LYP
Complex 1			Saddle point
Complex 2			
Complex 3			
Complex 4			
Complex 5			

Complex 5*		Saddle point	Saddle point
Complex 6			Saddle point
Complex 7			
Complex 8			
Complex 9			

Complex 10			
Complex 11			
Complex 12			
Complex 13			
Complex 1*	Saddle point	Saddle point	
Complex 4*	Saddle point		

Complex 1 is the global minimum obtained at M06-2X/6-311++G**. This conformer involves two hydrogen bonds; one of them involves the acidic hydrogen of formic acid approaching in a near perpendicular fashion to the π -electron density of the triple bond of acetylenic part, while the hydrogen attached to the carbon of formic acid approaches towards the π -electronic cloud of benzene ring. The O-H...C₁(AC) distance is 2.8 Å and O-H...C₂(AC) is 2.426Å on M06/6-311++G(d,p) level. These distances are consistent with typical hydrogen-bond interactions. For example, the hydrogen bond distances in the π -complex of acetylene with water is 2.443Å, at MP2/6-311++G (d, p) level [37]. For the second hydrogen bonded interaction, the distance between C-H (FA) to one of the phenyl carbons in PhA 2.792Å. This second interaction results in a cyclic structure and an additional stabilization of the complex. The global minimum structure obtained with the B3LYP method (complex 1*) is somewhat different from that obtained at the MP2 and M06-2X levels of theory. In this structure, there is only one interaction, which is between acetylenic π -cloud and O-H hydrogen of the formic acid. The Atoms-in-Molecule theory confirmed this single interaction by indicating a single (3,-1) bond critical point in the case of B3LYP, while at the MP2 and M06-2X levels, the two interactions lead to two (3,-1) bond critical points and a consequent (3,+1) ring critical point indicative of a cyclic structure.

The computed binding energies (ΔE), the BSSE-corrected ΔE , and the ZPE-corrected binding energies for Complex 1 is -7.5 kcal/mol, -6.7 kcal/mol, -6.6 kcal/mol respectively at M06-2X and -7.7,-7.5,-5.7 kcal/mol respectively on MP2 level. The uncorrected binding energy for Complex 1* is -4.3 kcal/mol and ZPE-corrected and BSSE-corrected energies are -3.7 kcal/mol and -3.9 kcal/mol respectively.

The geometries and interaction energies for other complexes are given in **Table 2** and **Table 3, 4, 5**.

Depending upon the situation, some of them have formed H- π bond, some n-sigma bond and rest of them form both kind of interactions.

Complex 1, 2, 3, 5, 6, 8 and 1* have H- π interactions. In these complexes, π -clouds of PhA (benzene and acetylene) act as proton acceptors and carboxylic hydrogen as well as the hydrogen attached to carbon of FA can act as proton donors.

Among the above complexes, Complex 1 and 2 have two H- π interactions forming a cyclic complex. Among the noncyclic geometries, benzene π -cloud acts as proton acceptors in Complex 5, 6 and 8 while acetylenic π -cloud in Complex 1* and 3. The typical distance between hydrogen and π -cloud is in the range of 2.5-2.9Å, which is in

Table 3 - Computed stabilization energy of the complexes at M06-2X/6-311++G (d, p)

Stabilization Energy at M06-2X/6-311++G(d,p)			
Complex	$\Delta E_{\text{Raw}}/\Delta E_{\text{ZPE}}/\Delta E_{\text{BSSE}}$ (kcal/mol)	Complex	$\Delta E_{\text{Raw}}/\Delta E_{\text{ZPE}}/\Delta E_{\text{BSSE}}$ (kcal/mol)
Complex 1	-7.5/-6.7/-6.6	Complex 7	-3.8/-3.3/-3.6
Complex 2	-7.1/-6.5/-6.3	Complex 8	-4.1/-3.4/-3.4
Complex 3	-6.1/-5.4/-5.6	Complex 9	-3.2/-2.7/-2.9
Complex 4	-5.9/-5.1/-5.6	Complex 10	-2.8/-2.1/-2.5
Complex 5	-5.5/-4.9/-4.8	Complex 11	-2.4/-2.1/-2.1
Complex 5*	-5.4/-4.9/-4.7	Complex 12	-2.3/-1.6/-1.8
Complex 6	-4.9/-4.2/-4.0	Complex 13	-1.8/-1.3/-1.5

Table 4 - Computed stabilization energy of the complexes at MP2/6-311++G (d, p)

Stabilization Energy at MP2/6-311++G(d,p)			
Complex	$\Delta E_{\text{Raw}}/\Delta E_{\text{ZPE}}/\Delta E_{\text{BSSE}}$ (kcal/mol)	Complex	$\Delta E_{\text{Raw}}/\Delta E_{\text{ZPE}}/\Delta E_{\text{BSSE}}$ (kcal/mol)
Complex 1	-7.7/-7.5/-5.7	Complex 8	-4.8/-4.2/-2.3
Complex 2	-7.7/-7.3/-4.6	Complex 9	-1.8/-1.2/-1.5
Complex 3	-6.6/-5.8/-4.6	Complex 10	-3.0/-2.7/-2.0
Complex 4	-5.8/-5.6/9.5	Complex 11	-1.6/-1.1/-1.4
Complex 4*	-3.0/-2.5/-2.0	Complex 12	-2.9/-2.1/-1.8
Complex 5	-6.4/-6.4/-4.6	Complex 13	-2.4/-1.7/-1.3
Complex 7	-3.5/-3.1/-2.4		

Table 5 - Computed stabilization energy of the complexes at B3LYP/6-311++G(d,p)

Stabilization Energy at B3LYP/6-311++G(d,p)			
Complex	$\Delta E_{\text{Raw}}/\Delta E_{\text{ZPE}}/\Delta E_{\text{BSSE}}$ (kcal/mol)	Complex	$\Delta E_{\text{Raw}}/\Delta E_{\text{ZPE}}/\Delta E_{\text{BSSE}}$ (kcal/mol)
Complex 1*	-4.3/-3.7/-3.9	Complex 8	-0.9/-0.7/-0.6
Complex 2	-3.3/-2.8/-2.6	Complex 9	-1.8/-1.2/-1.5
Complex 3	-3.9/-3.1/-3.5	Complex 10	-1.6/-1.1/-1.4
Complex 4	-3.8/-3.2/-2.6	Complex 11	-1.6/-1.1/-1.4
Complex 4*	-2.2/-1.5/-1.9	Complex 12	-1.6/-1.0/-1.2
Complex 5	-2.4/-1.9/-1.9	Complex 13	-1.3/-0.7/-1.0
Complex 7	-2.2/-1.6/-2.1		

good agreement with the literature [11].

The geometries in which n-sigma is the dominating interaction are Complex 4*, 10, 12 and 13. In these complexes, the terminal hydrogen of the acetylene moiety of PhA acts as proton donor while hydroxyl and carbonyl oxygen of FA act as proton acceptor. In Complex 4* and 10, carbonyl oxygen acts as proton acceptor while in Complex 12 and 13, hydroxyl oxygen does the same role. The bond distances were computed to be in the range of 2.2 - 2.4 Å.

There are also some structures where both H- π and n-sigma, interactions are present. Complex 4, 7, 9 and 11 fall in this category. In Complex 4 and 7, acetylenic hydrogen acts as one of the proton donors while in Complex 9 and 11, hydrogen attached to benzene ring participate in n-sigma bond formation. Both monomers are in plane in Complex 9 and 11 while they are perpendicular in Complex 4 and 7.

3.4 Vibrational Analysis:

The vibrational frequencies of the monomers and their complexes have been computed at M06-2X (**Table 6**), MP2 (**Table 7**) and B3LYP (**Table 8** and **9**) level using 6-311++G (d, p) basis set. At M06-2X and MP2 level, Complex 1 is the most stable one, while Complex 1* is the most stable at the B3LYP level.

In the complex 1, the O-H stretching mode in FA shows a large red shift. At the M06-2X level, this mode appears at 3898.43 cm^{-1} in the monomer while in the complex it appears at 3835.7 cm^{-1} which amounts to a red shift of 63 cm^{-1} in the complex. At the MP2 level, the red shift for this mode has been computed to be 78 cm^{-1} . The other vibrational modes with significant shifts are C=O stretch in FA at 1900.2 cm^{-1} , ($\Delta\nu = 27\text{cm}^{-1}$) the C-H stretch in PhA as 3466.2 cm^{-1} ($-\Delta\nu = 30\text{ cm}^{-1}$). At the MP2 level, the C=O stretch appears at 1828.4 cm^{-1} which is red shifted by 17 cm^{-1} from the monomer frequency and the C-H stretching frequency of phenylacetylene at 3488.9, with a red shift of 10 cm^{-1} . The frequency shift for C-O-H bend and C-O stretch is relatively small with red shifts of 5 cm^{-1} and blue shifts of 3 cm^{-1} . However, the small shifts are also detectable in the matrix isolation IR experiments, if these complexes are formed in the matrix. All the other modes are negligibly perturbed. At MP2 level, C-H stretch of formic acid is blue shifted by 14 cm^{-1} while at M06-2X level of calculation no shift is observed. The C-H bend at both levels is difficult to be detected since it is shifted by 1 cm^{-1} . The computed spectra of Complex 1 at M06-2X level is shown below in **Figure 8 (a), (b) and (c)**.

Table 6 - Computed frequencies of the monomers and the complexes at M06-2X/6-311++G (d, p)

Computed Frequencies								
M06-2X/6-311++G (d, p)								
Monomer (1,2) ^a	Complex 1	Complex 2	Monomer (3,4,5,5*)	Complex 3	Complex 4	Complex 5	Complex 5*	mode of assignment
3898.43	3835.7(-63)	3839.5(-59)	3814.4	3668.2(-146)	3672.3(-142)	3571.7(-242)	3743.3(-71)	O-H stretch
3050.9	3050.6(0)	3045.5(-5)	3120.1	3115.7(-4)	3120.5(0)	3115.7(-4)	3118.3(-2)	C-H stretch
1927.72	1900.2(-27)	1909.3(-18)	1875.6	1862.1(-13)	1860.8(-15)	1865.8(-10)	1863.2(-12)	C=O stretch
1136.43	1139.9(3)	1148.4(12)	1169.6	1199.1(29)	1202.7(33)	1175.2(6)	1177.5(8)	C-O stretch
3496.14	3466.2(-30)	3477.8(-18)	3496.1	3473.3(-23)	3452.4(-44)	3486.4(-10)	3476.5(-19)	C-H stretch PhA
1297.74	1292.2(-5)	1297.7(-1)	1317.6	1338.1(20)	1356.0(38)	1318.6(1)	1321.8(4)	O-H bend
1441.86	1440.7(-1)	1444.6(3)	1415.3	1428.1(13)	1425.4(10)	1418.3(3)	1424.3(9)	C-H bend

^amonomer (a, b) represents monomer of complex a and b

Table 7 - Computed frequencies of the monomers and the complexes at MP2/6-311++G (d, p)

Computed Frequencies							
MP2/6-311++G (d, p)							
Monomer (1,2) ^a	Complex 1	Complex 2	Monomer (5,3,6)	Complex 5	Complex 3	Complex 6	mode of assignment
3862.7	3784.8(-78)	3800.1(-62)	3797.8	3737.9(-60)	3662.9(-135)	3791.6(-6)	O-H stretch
3034.5	3048.3(14)	3048.4(14)	3130.8	3114.6(-16)	3115.0(-16)	3127.6(-3)	C-H stretch
1845.0	1828.4(-17)	1829.6(-15)	1808.8	1796.7(-12)	1794.2(-15)	1800.3(-8)	C=O stretch
1117.5	1129.1(12)	1130.1(12)	1142.1	1150.4(8)	1170.6(28)	1138.6(-4)	C-O stretch
3498.7	3488.9(-10)	3493.6(-5)	3498.7	3497.4(-1)	3489.1(-10)	3496.2(-2)	C-H stretch PhA
1293.45	1307.9(14)	1297.0(3)	1311.31	1315.7(4)	1335.9(24)	1315.7(4)	O-H bend
1447.69	1448.6(1)	1446.2(-1)	1429.2	1432.9(4)	1432.9(4)	1432.9(4)	C-H bend

^amonomer (a, b) represents monomer of complex a and b

Table 8 - Computed frequencies of the monomers and the complexes at B3LYP/6-311++G (d, p)

Computed Frequencies							
B3LYP/6-311++G (d, p)							
Monomer (1*,2,7) ^a	Complex 1*	Complex 2	Complex 7	Monomer (3,4)	Complex 3	Complex 4	mode of assignment
3799.8	3645.1(-154)	3725.4(-74)	3799.3(-1)	3738.3	3576.1(-162)	3572.1(-166)	O-H stretch
2961.1	2963.8(3)	2975.5(14)	2974.7(14)	3056.8	3045.6(-11)	3044.7(-12)	C-H stretch
1860.8	1846.1(-15)	1847(-14)	1849.2(-12)	1816.7	1797.5(-19)	1797.4(-19)	C=O stretch
1099.0	1128.8(30)	1112.4(13)	1112.0(13)	1124.9	1156.2(31)	1159.6(34)	C-O stretch
3476.4	3464.5(-12)	3472.4(-4)	3409.1(-67)	3476.4	3466.1(-10)	3451.9(-24)	C-H stretch PhA
1269.35	1308.5(39)	1278.3(9)	1274.4(5)	1292.9	1318.3(25)	1325.5(33)	O-H bend
1419.27	1419.8(1)	1421.6(2)	1421.7(2)	1403.4	1409.5(6)	1412.1(9)	C-H bend

^amonomer (a, b) represents monomer of complex a and b

Table 9 - Computed frequencies of the monomers and the complexes at B3LYP/6-311++G (d, p)

Calculated Frequencies					
B3LYP/6-311++G (d, p)					
Monomer (10) ^a	Complex 10	Monomer (4*,5)	Complex 4*	Complex 5	mode of assignment
3799.8	3798.6(-1)	3738.3	3735.0(-3)	3654.6(-84)	O-H stretch
2961.1	2975.5(14)	3056.8	3066.2(9)	3047.3(-9)	C-H stretch
1860.8	1852.5(-8)	1816.7	1805.0(-12)	1804.7(-12)	C=O stretch
1099.0	1110.3(11)	1124.9	1138.5(14)	1145.4(20)	C-O stretch
3476.4	3419.8(-56)	3476.4	3413.4(-63)	3474.7(-2)	C-H stretch PhA
1269.35	1271.9(2)	1292.9	1301.0(8)	1309.4(16)	O-H bend
1419.27	1419.7(0)	1403.4	1404.1(1)	1408.9(5)	C-H bend

^amonomer (a, b) represents monomer of complex a and b

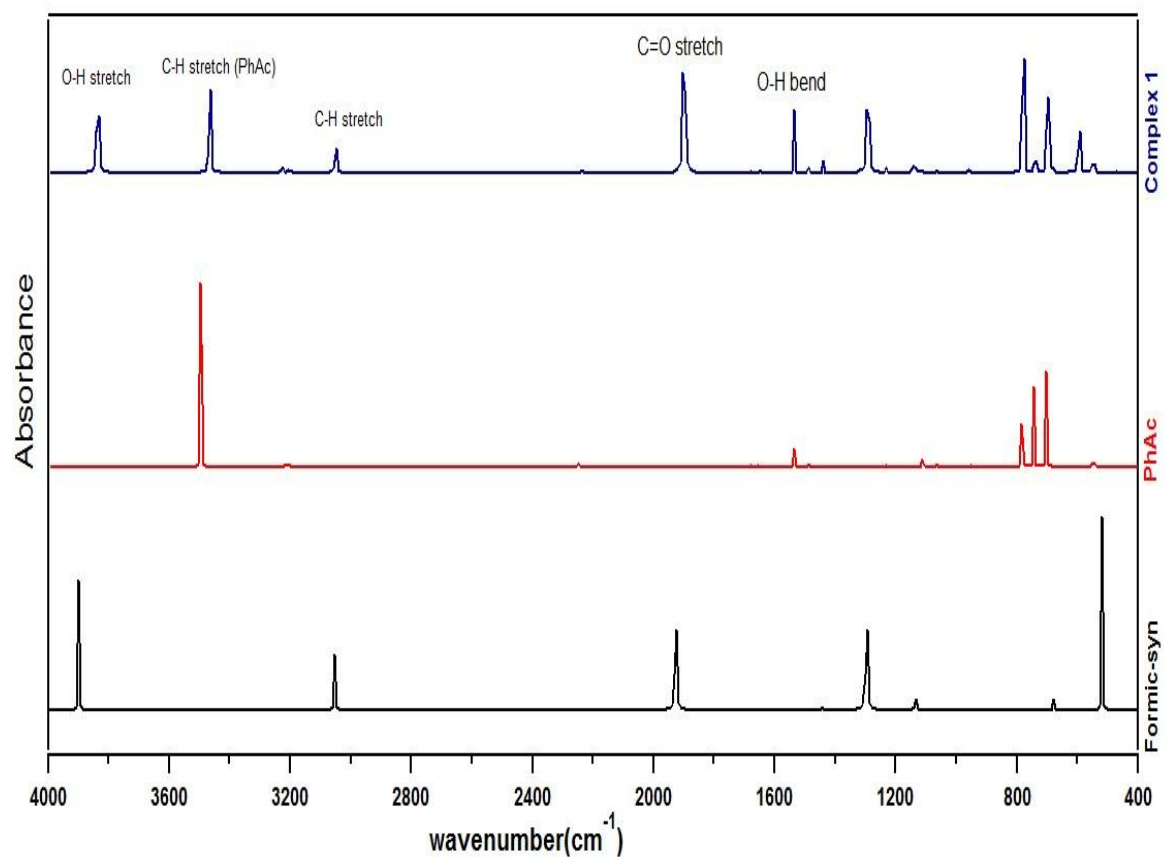


Figure 8 (a) - Computed spectrum of Complex 1 at M06-2X/6-311++G (d, p);

Scale : (4000 - 400 cm^{-1})

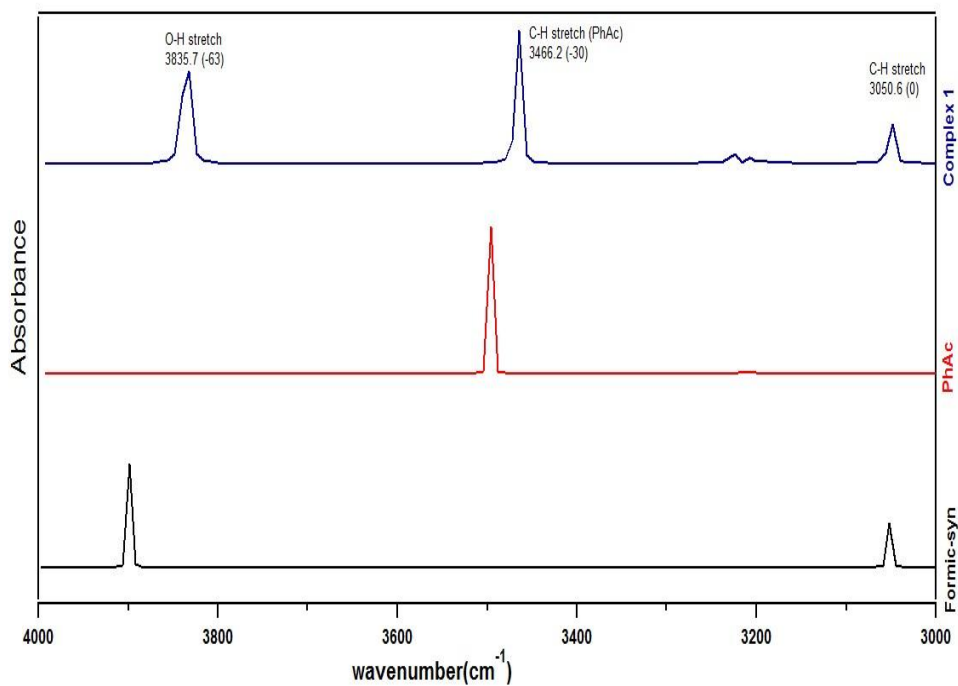


Figure 8 (b) - Computed spectrum of Complex 1 at M06-2X/6-311++G (d, p);
Scale: (4000 – 3000 cm⁻¹)

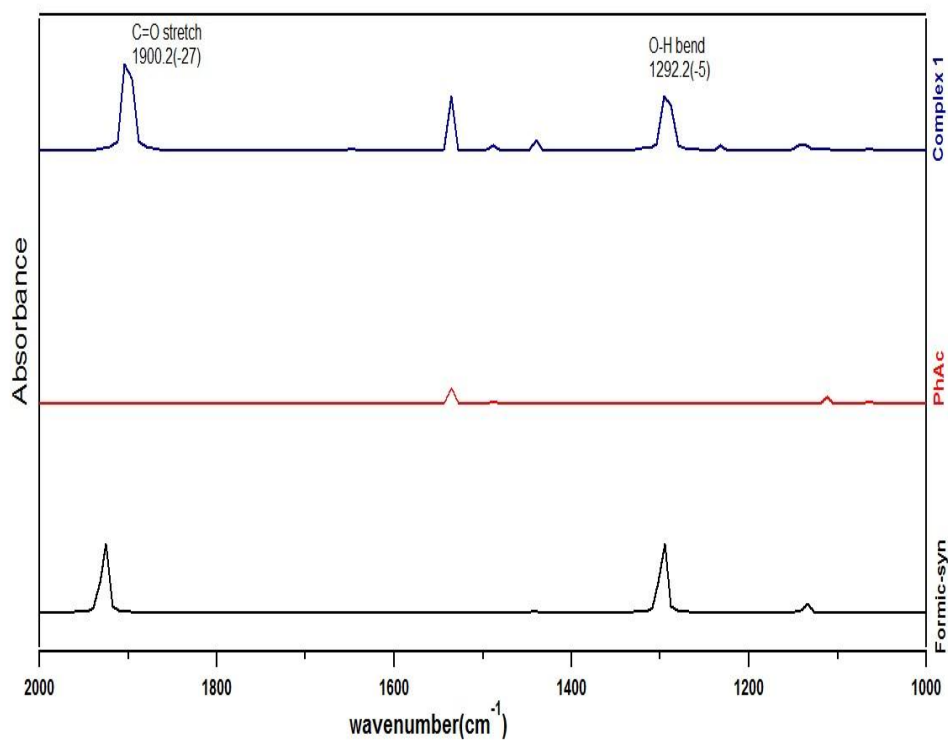


Figure 8 (c) - Computed spectrum of Complex 1 at M06-2X/6-311++G (d, p);
Scale: (2000 – 1000 cm⁻¹)

At B3LYP level, Complex 1* is the ground state geometry. Here, the O-H $\cdots\pi$ interaction is the dominant interaction. The computed spectra for Complex 1* is shown in **Figure 9 (a), (b) and (c)**. The O-H stretch appears at 3799.8 cm⁻¹ in the monomer while in the complex the feature is observed at 3645.1 cm⁻¹, resulting in a large shift of 154 cm⁻¹. Since, O-H group has participated in bond formation; the C-O-H bending is also blue shifted by 39 cm⁻¹. The other significantly perturbed vibrational modes are C-O stretch and C=O stretch appearing at 1128.8 cm⁻¹ and 1846.1 cm⁻¹, with a blue shift of 30 cm⁻¹ and a red shift of 15 cm⁻¹ respectively. The C-H stretch in PhA is red-shifted by 12 cm⁻¹. The C-H mode in formic acid is largely unperturbed, probably because of the large distance between the π -cloud of phenylacetylene and the C-H group of formic acid.

While doing the experiment, two methods of sample introduction will be employed. In first method, both monomers will be mixed in the mixing chamber with the inert gas before deposition. Here, complexes may form prior to deposition and the population distribution of the complexes will depend on the room temperature (298 K) energy. In second method, monomers will be separately introduced in the vacuum system for the deposition. Then the matrix will be annealed to allow the monomers to diffuse and come close to each other to form complex. The population distribution of the complexes will depend upon the annealing temperature. Among the two methods of formation of complex, the more stable complex is likely to have a larger population in the first method, where the complexes are formed at room temperature, and will be dictated by the Boltzmann population distribution. Both methods will be attempted. In this report, the computed vibrational frequencies (**Table 6, 7, 8 and 9**) for a few complexes have been presented. Experiments will reveal which of these are formed in the matrix.

In adducts, one of the monomers is formic acid. It exists in two forms; syn and anti, which are defined by the rotation of the OH group around the C-O bond. The experimental relative energy difference of 3.97 kcal/mol between the two conformers [38] is inserted into the Boltzmann equation to estimate the population ratio between the anti and syn rotamers. At 298 K, the value obtained is 1.2×10^{-3} . This small population of syn-HCOOH in the gas phase explains why it is hard to detect it with IR. But Hocking and Bjarnov [39] detected syn-formic acid by using microwave spectroscopy.

In matrix isolation IR spectroscopy, different conformations of a molecular complex are trapped provided the conformers have detectable populations in the gas phase.

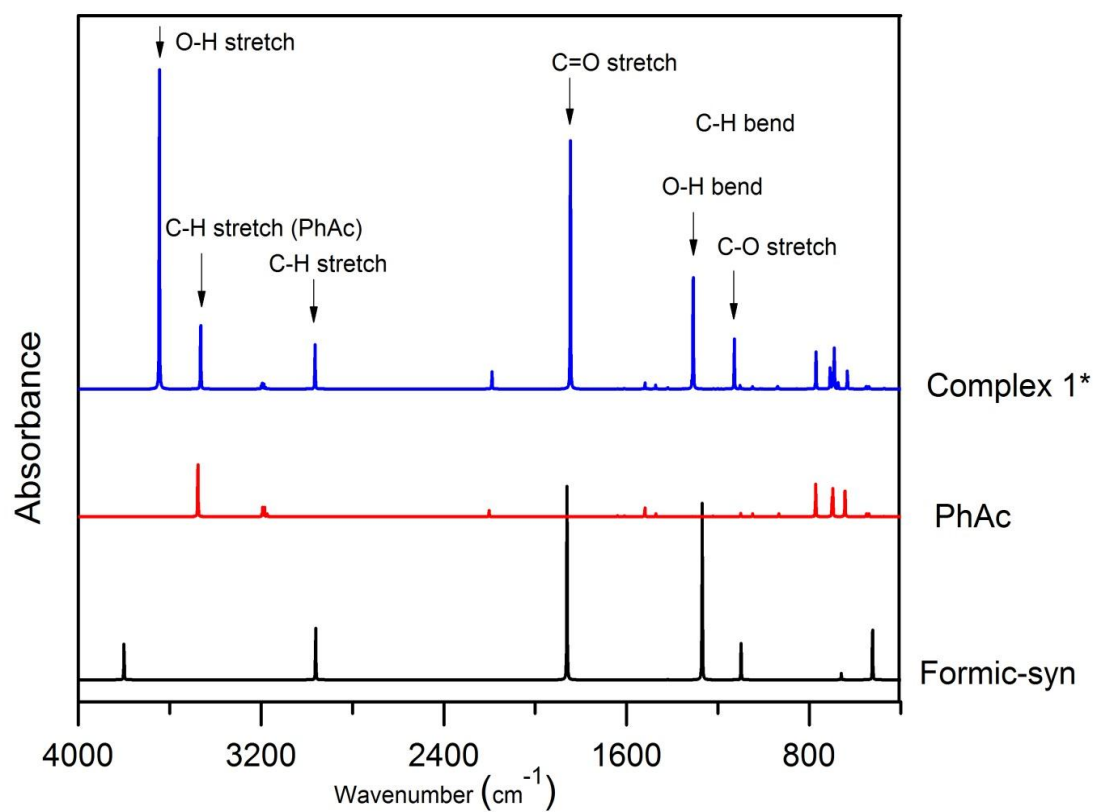


Figure 9 (a) - Computed IR spectra of the Complex 1* at B3LYP/6-311++G (d, p);
Scale: (4000 – 400 cm^{-1})

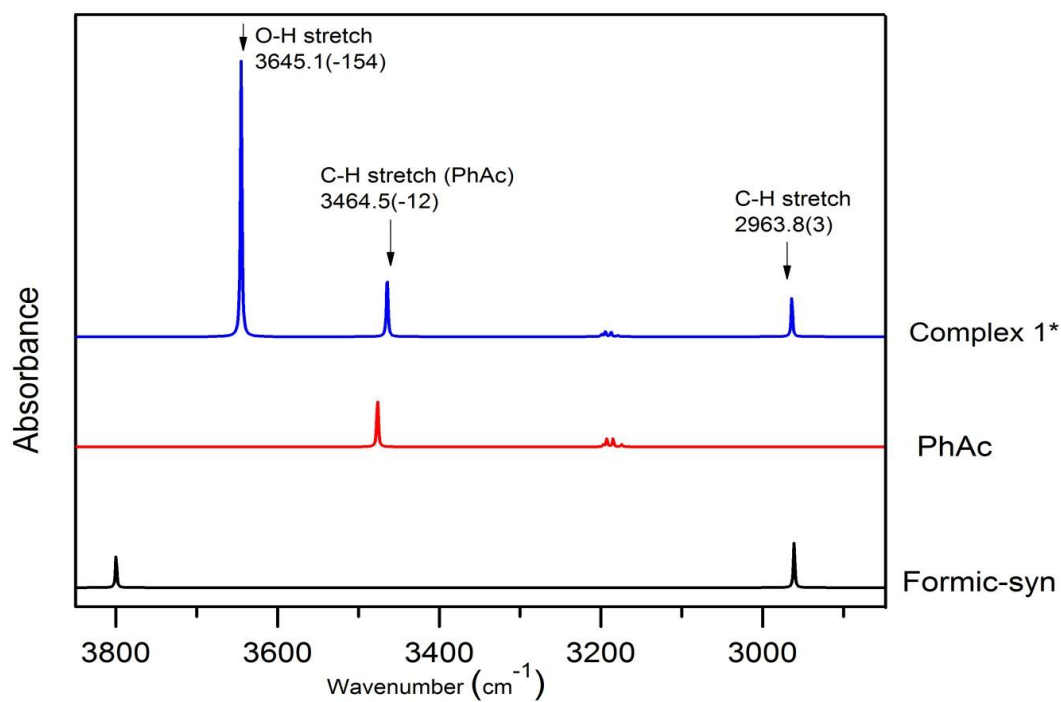


Figure 9 (b) - Computed IR spectra of the Complex 1* at B3LYP/6-311++G (d, p);
Scale: (3850- 2850)

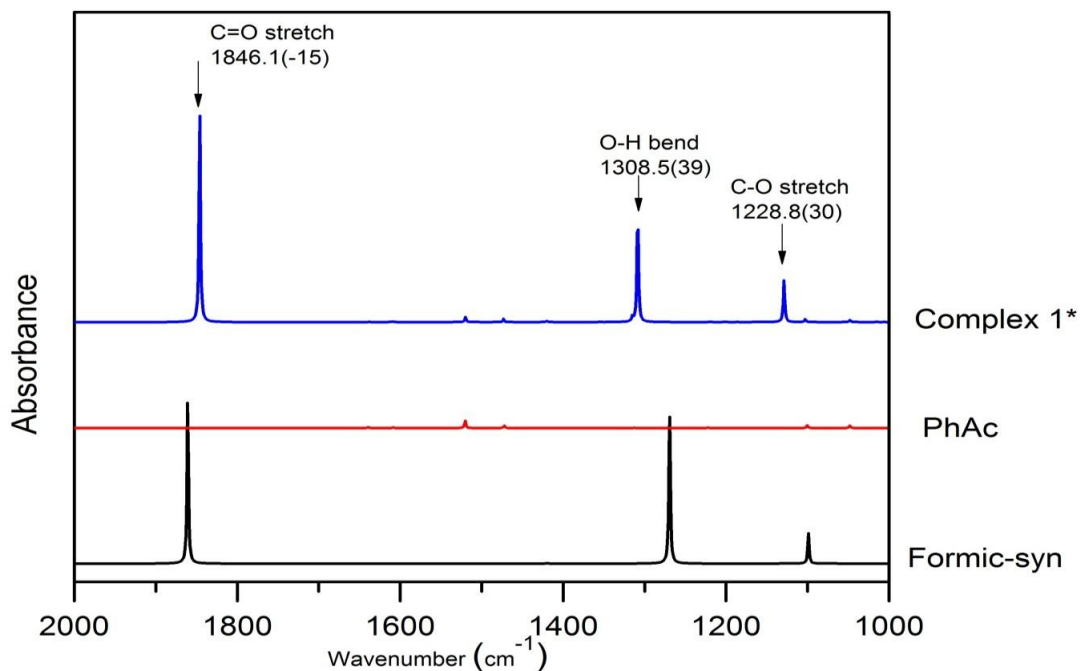


Figure 9 (c) - Computed IR spectra of the Complex 1* at B3LYP/6-311++G (d, p);
Scale: (2000 – 1000 cm^{-1})

Using the matrix isolation facility that was built, the spectrum of phenylacetylene has been recorded, and is compared with the spectrum of liquid phenylacetylene. In **Figure 10 (a) and (b)**, it is very clear that the spectral features in matrix isolation facility are sharp, which is one of the major advantages of this experimental technique.

In the above spectrum, peak at 3323 and 3056 cm^{-1} is due to the C-H stretch of terminal acetylenic part and the benzene ring respectively. The arrow shows an additional feature which appears after annealing.

3.5 Geometrical parameters

The bond parameters are indicators to confirm a bond formation and explain magnitudes of frequency shift. The changes in geometrical parameters of complexes at M06-2X level are shown below. Recently, a vast amount of literature supports the use of M06-2X level of theory for weak interactions. The selected geometrical parameters have been shown in the **Table 10**. Atomic numbers in the complexes shown in **Table 10** can be viewed from **Figure 11**.

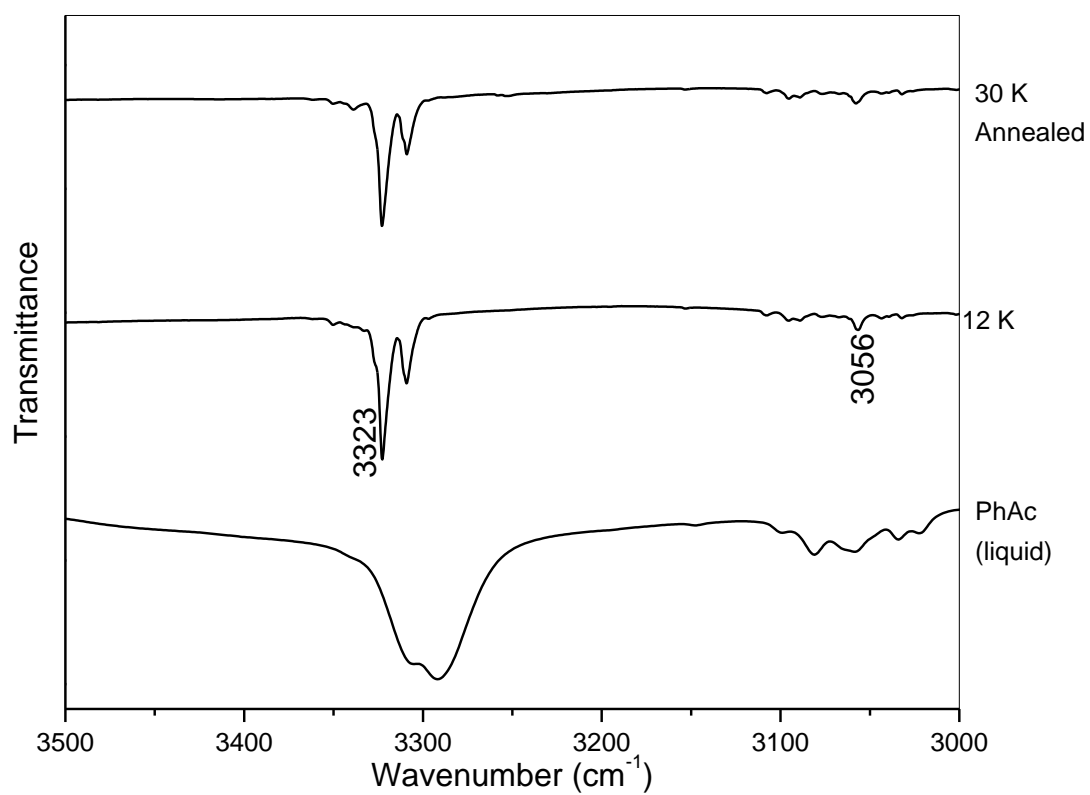


Figure 10 (a) - Spectrum of phenylacetylene recorded in liquid state and in matrix;
Scale: (3500-3000 cm^{-1})

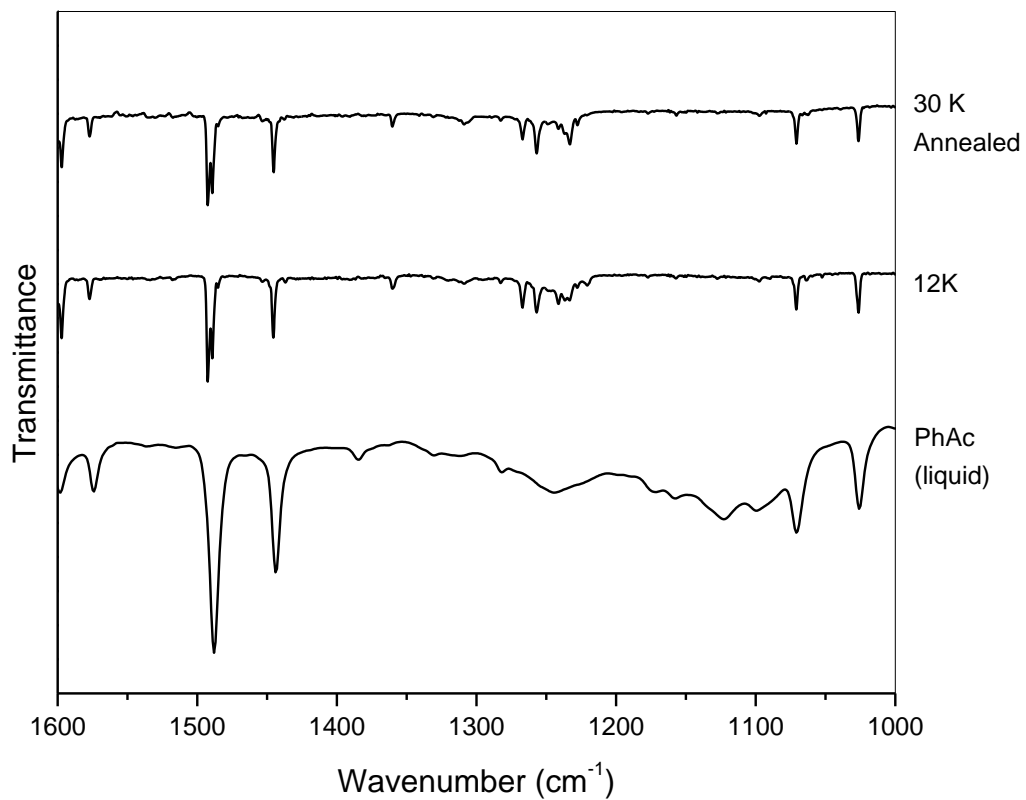


Figure 10 (b) - Spectrum of phenylacetylene recorded in liquid state and in matrix;
Scale: (1600 -1000 cm^{-1})

Table 10 - Some selected geometrical parameters at M06-2X /6-311++G (d, p)

Parameters	Formic syn	Formic anti	Complex 1	Complex 2	Complex 3	Complex 4	Complex 5
r(O-H) ^a	0.962	0.969	0.966	0.966	0.975	0.975	0.972
r(C-O)	1.345	1.350	1.343				
r(C=O)	1.186	1.198	1.102		1.197	1.198	1.196
r(C-H)	1.103	1.074		1.103			
<(COH) ^b	110.2	112.6	110.7		109.2	108.4	108.8
<(O=CO)	122.5	124.6			125.4	125.3	
<(O=CH)	123.7	125.8					
r(C=C) Ph ^c	1.202		1.202				
r(H15-C3)			2.426		2.280		
r(H15-C2)			2.800		2.312		
r(H19-C4)			2.792				
r(H19-C9)			3.103				
r(H19-C3)				2.819			
r(H19-C2)				3.323			
r(H15-C4)				2.689			2.822
r(H15-C9)				2.687			2.551
r(H14-O15)						2.644	
r(H19-C13)						2.252	
r(H19-C12)						2.346	
r(C5-O18)							3.033

^ar = Bond distance in Å,^b< = Bond angle in deg,^cph = Phenylacetylene

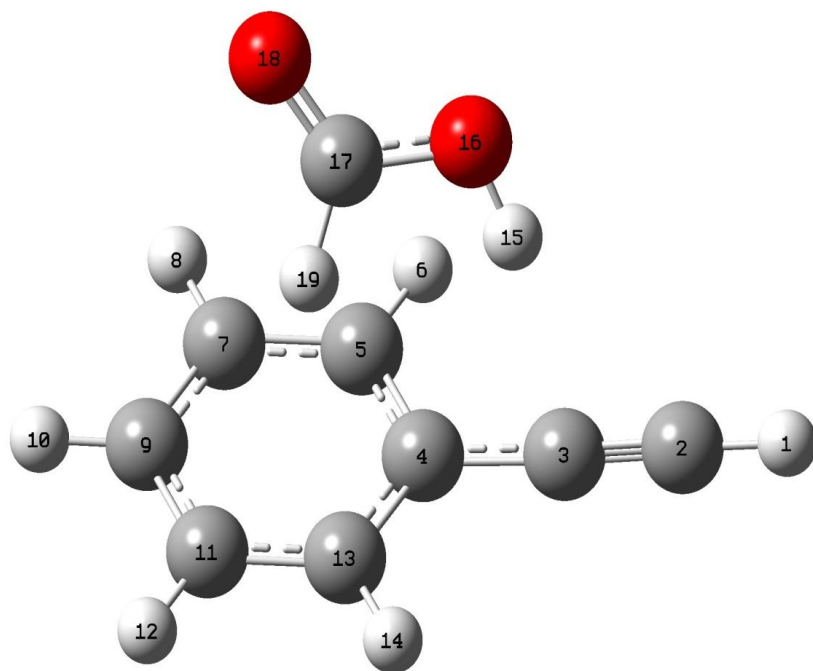


Figure 11 - Optimized geometry of Complex 1 at M06-2X/6-311++G (d, p)

Chapter 4

Conclusion

The thesis provides a computational study of weak interactions between formic acid and phenylacetylene. The computational study has been performed by GAUSSIAN 09 [23] suite of programmes. The computational analysis has been carried out at M06-2X, MP2, B3LYP levels of theory using a 6-311++G(d,p) basis set. In total, formation of sixteen different complexes has been revealed between the two monomers. Fourteen different geometries were obtained at M06-2X level while MP2 and B3LYP yielded twelve and thirteen structures, respectively. Many of the structures turned out to be similar in the three levels of theory. The ground state geometry of the formic acid-phenylacetylene complexes is almost same on M06-2X and MP2 level, which is Complex 1. At B3LYP level, the geometry of the ground state is different from the structures obtained above and is denoted as complex 1*. The BSSE corrected stabilization energy for the Complex 1 is -6.6 and -5.7 kcal/mol at M06-2X and MP2 level, respectively. The BSSE corrected stabilization energy for ground state (Complex 1*) at B3LYP level is -3.9 kcal/mol. It has been analyzed computationally that there are two interactions possible in global minimum structure obtained at the M06-2X and MP2 levels. One involves the interaction between acidic hydrogen of formic acid and acetylenic π cloud of phenylacetylene and another between the hydrogen attached to carbon of formic acid and benzene π cloud. The cyclic geometry of the complex has been confirmed by Atoms in Molecule theory, which showed a ring critical point. At B3LYP level, the main interaction is between acidic hydrogen of formic acid and acetylenic π -cloud. Vibrational frequency calculation revealed that the most perturbed mode is the O-H stretch of formic acid in Complex 1 and Complex1*. The other vibrational modes, which showed significant shifts are C=O stretch of formic acid, and C-H stretch of phenylacetylene, both of which showed red shifts, at the M06-2X and MP2 level, while the C-O-H bend showed a blue shift, at the B3LYP level.

The setting up of the matrix isolation infrared facility, to study the weak interactions between the two monomers, is also described, which is a major contributions

of this work. The matrix isolation facility consists of a cryostat, which provides low temperature upto 12 K and a vacuum system, which uses a diffusion pump to achieve a low pressure in the order of 10^{-6} mbar. A cold cathode gauge was used to measure the pressure in the range of 10^{-6} mbar while a Pirani gauge was used to measure pressure in the range of 10^{-2} mbar. A double jet nozzle was used to introduce the sample into the vacuum system. As matrix isolation experiments are known to trap local minima, it would be interesting to probe how many of the computed complexes of the phenylacetylene-formic acid can be observed in the matrix isolation experiments.

Bibliography

1. http://en.wikipedia.org/wiki/Chemical_bond
2. “*The Chemical bond : Structure and Dynamics*” edited by Ahmed Zewail, Academic Press
3. Moore, T. S.; Winmill, T. F. *J. Chem. Soc.* 1919, 41, 868–1543.
4. Desiraju, G. R.; Steiner, T. *The Weak Hydrogen Bond: In Structural Chemistry and Biology*, Oxford Science Publication.
5. Arunan, E; Desiraju, G.R; Klein, R, A; Sadlej,J ; Scheiner,S; Alkorta, I; Clary, D.C; Crabtree,R.H; Dannenberg, J.J; Hobza, p; Kjaergaard, H.G; Legon, A.C; Mennucci, B; Nesbitt;D.J. *Pure Appl. Chem.* 2011, 83, 1619
6. Legon, A. C.; Millen, D. J. *Chemical Society Reviews*, 16,467-98, [127,414]
7. Scheiner, S.; *Hydrogen bonding. A theoretical perspective.* Oxford University press, Oxford. 1997, [4,21,27,80,171]
8. Jeng, M. H.; Delaat, A. M.; Ault, B. S. *J. Phys. Chem.* 1989, 93, 3997
9. Delaat, A. M.; Ault, B. S. *J. Am. Chem. Soc.* 1987, 109, 4232
10. Hartmann, M; Wetmore, S. D.; Radom, L. *J. Phys. Chem. A.* 2001, 101, 4470.
11. George, L; Garcia, E; Sander, W; *J. Phys. Chem. A* 2003,107, 6850-6858
12. George, L; Sander, W. *Spectrochimica Acta Part A* 2004, 60, 3225–3232
13. Marushkevich, K; Khriachtchev, I; Lundell, J; Domanskaya,A; Rasanen, M. *J. Phys. Chem. A* 2010, 114, 3495–3502
14. <http://webbook.nist.gov/chemistry>
15. Singh, P. C.; Bandyopadhyay, B; Patwari, G. N. *J. Phys. Chem. A* 2008, 112, 3360
16. Maity, S; Guin, M; Singh, P. C; Patwari, G.N. *Chem. Phys. Chem.* 2011, 12, 26-46
17. Maity, S; Patwari, G.N; Sedlak, R; Hobzq, P. *Phys. Chem. Chem. Phys.* 2011, 13, 16706
18. Whittle, E; Dows, D. A; Pimentel, G. C. *J. Chem. Phys.* 1954, 22, 1943
19. Hallam, H. E. *Vibrational Spectroscopy of Trapped Species* (Wiley Inter science Publication, London, 1973)

20. Cradock, S.; Hinchcliffe, A. J. *Matrix Isolation, Chap. 2*, Cambridge University Press, London (1975).
21. Pimentel, G. C; Charles, S. W. *Pure and Appl. Chem.* 1963, 7, 111
22. Buckingham, A. D. *Proc. Roy. Soc. (London) A* 1958, 248, 169
23. Hastie, W.; Hauge, R. H. ; Margrave, J. L. *Spectroscopy in inorganic chemistry* 1970, 1, 57, Academic Press, New York
24. Moskovits, M. ; Ozin, G. A. ; *Cryochemistry, Chap 2*, Wiley Inter science Publication, New York (1976)
25. Barnes, A. J.; Hallam, H. E. *Quarterly Reviews*, Chemical Society (London), 1969, 23, 392
26. www.arscryo.com
27. Griffiths, P. R.; Haseth, J. A : *Fourier Transform Infrared Spectrometry* (John Wiley & Sons), New York, 1986
28. Gaussian 09, Revision A.1, Frisch, M. J.; Trucks, G. W.; Schlegel, H. B.; Scuseria, G. E.; Robb, M. A.; Cheeseman, J. R.; Scalmani, G.; Barone, V.; Mennucci, B.; Petersson, G. A.; Nakatsuji, H.; Caricato, M.; Li, X.; Hratchian, H. P.; Izmaylov, A. F.; Bloino, J.; Zheng, G.; Sonnenberg, J. L.; Hada, M.; Ehara, M.; Toyota, K.; Fukuda, R.; Hasegawa, J.; Ishida, M.; Nakajima, T.; Honda, Y.; Kitao, O.; Nakai, H.; Vreven, T.; Montgomery, Jr., J. A.; Peralta, J. E.; Ogliaro, F.; Bearpark, M.; Heyd, J. J.; Brothers, E.; Kudin, K. N.; Staroverov, V. N.; Kobayashi, R.; Normand, J.; Raghavachari, K.; Rendell, A.; Burant, J. C.; Iyengar, S. S.; Tomasi, J.; Cossi, M.; Rega, N.; Millam, J. M.; Klene, M.; Knox, J. E.; Cross, J. B.; Bakken, V.; Adamo, C.; Jaramillo, J.; Gomperts, R.; Stratmann, R. E.; Yazyev, O.; Austin, A. J.; Cammi, R.; Pomelli, C.; Ochterski, J. W.; Martin, R. L.; Morokuma, K.; Zakrzewski, V. G.; Voth, G. A.; Salvador, P.; Dannenberg, J. J.; Dapprich, S.; Daniels, A. D.; Farkas, Ö.; Foresman, J. B.; Ortiz, J. V.; Cioslowski, J.; Fox, D. J. Gaussian, Inc., Wallingford CT, 2009.
29. F. Biegler-König, R. F. W. Bader, W. -H. Tang, *J. Comput. Chem.* 2000, 96, 6796, AIM 2000
30. A. D. Becke, *Phys. Rev. A* 1989, 38, 3098
31. A. D. Becke, *J. Chem. Phys.* 1983, 98, 5648
32. Scuseria, G. E.; Staroverov, V. N. *Theory and Application of Computational Chemistry: the first forty years*. Elsevier, 669-724
33. Zhao, Y.; Truhlar, D. G. *Theor Chem Account* 2008, 120, 215-241

34. Boys, S. F.; Bernadi, F.; *Mol. Phys.* 1970 , 19, 553
35. R. F. W. Bader, *Atoms in Molecules. A Quantum Theory*, Clarendon Press, Oxford, 1994
36. R. M. Bentwood, A. J. Barnes, W. J. Orville-Thomas. *J. Mol. Spectrosc.* 1980, 84, 391
37. Grabowski, S. J. *J. Phys. Chem. A.* 2001, 105, 10739
38. Bjarnov, E.; Hocking, W. M. *Z. Naturforsch.* 1978, 33A, 610
39. Hocking, W. M. *Z. Naturforsch.* 1976, 31A, 1113

Poster Presentations / Publications

- ❖ *Phenylacetylene – Formic Acid Hydrogen Bonded Complexes: A Computational and Matrix Isolation IR study*: Gaurav Kumar.; Bishnu Prasad Kar.; K. S. Viswanathan, Poster Presented, 3rd Indo-German Conference on Modeling Chemical and Biological Re-activity (MCBR3), 26th Feb. – 1st Mar. 2013